Enhanced Evaluation of hourly and Daily Extreme Precipitation in Norway from Convection-Permitting Models at Regional and Local Scales

Kun Xie[1,2], Lu Li[3], Hua Chen[1,2], Stephanie Mayer[3], Andreas Dobler[4], Chong-Yu Xu[5], Ozan Mert Gokturk[3]

[1]State Key Laboratory of Water Resources and Hydropower Engineering Science, Wuhan University, Wuhan

430072, P. R. China

[2]Hubei Provincial Key Lab of Water System Science for Sponge City Construction, Wuhan University, Wuhan,

China

[3]NORCE Norwegian Research Centre, Bjerknes Centre for Climate Research, Bergen, Norway

[4]The Norwegian Meteorological Institute, Oslo, Norway

[5]Department of Geosciences, University of Oslo, P.O Box 1047 Blindern, 0316 Oslo, Norway

Correspondence to: Hua Chen (chua@whu.edu.cn); Lu Li (luli@norceresearch.no)

Abstract

Convection-permitting regional climate models (CPRCMs) have demonstrated enhanced capability in capturing extreme precipitation compared to regional climate models (RCMs) with convection-parameterization schemes. Despite this, a comprehensive understanding of their added values in daily or sub-daily extremes, especially at local scale, remains limited. In this study, we conduct a thorough comparison of daily and sub-daily extreme precipitation from the HARMONIE-Climate (HCLIM) model at 3 km resolution (HCLIM3) and 12 km resolution (HCLIM12) across Norway's diverse landscape, divided into five regions, using both gridded and in-situ observations. Our main focus is to investigate the added value of CPRCMs (i.e., HCLIM3) compared to RCMs (i.e., HCLIM12) for extreme precipitation at daily and sub-daily scales from regional to local scales, and quantify to what extend CPRCMs can reproduce the orographic effect on extreme precipitation at daily and sub-daily scale. We find that HCLIM3 better matches observations than HCLIM12 for daily and hourly extreme precipitation across all grid points in Norway, while HCLIM12 underestimates the extremes, especially for hourly extremes. At the regional scale, HCLIM3 captures the maximum 1-day precipitation (Rx1d) and maximum 1-hour precipitation (Rx1h) more accurately across most regions and seasons, except summer. Besides, HCLIM12 underestimates daily return levels across most regions while HCLIM3 shows larger bias of daily extreme in the east and west at the local scale. Nevertheless, HCLIM3 consistently demonstrates added value in simulating daily extremes in the middle and north regions at both regional and local scales, as well as hourly extremes at all 10 stations, compared with HCLIM12. Both HCLIM3 and

33 HCLIM12 capture the seasonality of extreme precipitation well across most regions, with HCLIM3 outperforming
34 HCLIM12 for hourly extremes. Additionally, the reverse orography effect on seasonal Rx1h and Rx1d is well
35 captured, with HCLIM3 showing added value in representing the reverse orographic effect of daily extremes except
36 in summer. This study highlights the importance of more realistic convection-permitting regional climate
37 simulations in providing reliable insights into the characteristics of precipitation extremes across Norway's five
38 regions. Such information is crucial for effective adaptation management to mitigate severe hydro-meteorological
39 hazards, especially for the local extremes.

40 **1 Introduction**

41 In recent years, the world has witnessed a surge in both frequency and intensity of floods primarily attributed to the
42 increasing occurrence of intensive rainfall events (Tabari, 2020). These changes underscore the pressing need to
43 develop a predictive understanding of precipitation extremes for the upcoming decades, given the ongoing globe
44 warming. The intensification of precipitation extremes under the influence of global warming has the potential to
45 trigger severe natural hazards and exert significant socioeconomic impacts (Thackeray et al., 2022), which has
46 gained substantial attention in recent research endeavors. However, most previous research in this field relied on
47 coarse-resolution GCMs with grid sizes exceeding 100 km, which struggle to accurately simulate extreme
48 precipitation events and their frequency due to the limitations of their coarser resolution (Piani et al., 2010; Wang et
49 al., 2017). Notably, these GCMs tend to produce the largest errors in predicting extreme precipitation, particularly in
50 cases involving heavier convective activity, as observed in the study by Gervais et al. (2014a). Despite various bias-
51 correction techniques are applied to mitigate these discrepancies on the GCMs, as well as employing them as forcing
52 data for regional climate models (RCMs) with grid size larger than 10 km, it remains a persistent challenge to
53 eliminate the transfer of biases from GCMs to RCMs, as noted by studies such as Pontoppidan et al. (2018) and Kim
54 et al. (2020). The large resolution gap between GCMs or RCMs and localized precipitation extremes further
55 constrains the robust simulations of extreme precipitation as highlighted by Li et al. (2020a). In addition, the
56 reliance on parameterization schemes to represent convection in these coarse resolution models introduces a
57 significant source of uncertainty in modelling errors (Prein et al., 2015; Kendon et al., 2019). More frequent and
58 intense precipitation events under global warming stimulate interest in higher resolution and physics-based models
59 to improve the estimation of short-duration extremes.

60   Convection-permitting regional climate models (CPRCMs), with grid size of less than 4 km, offer a promising
61 alternative, which explicitly represent convection, eliminating the need for parameterizations of deep atmospheric
62 convection. The potential in resolving deep convection and local extremes from CPRCMs lead to the realistic
63 representation in daily and sub-daily precipitation features, including diurnal cycle, intensity and frequency of heavy
64 precipitation events, seasonality, spatial-temporal pattern, wet-spell and dry-spell. For instance, CPRCMs have been
65 proven to reduce the bias and enhance the representation in precipitation intensity and intensity in the Tibetan
66 Plateau, the highest highland in the world, as shown in Li et al. (2021). In addition to their capability in capturing
67 precipitation, Liu et al. (2017) also demonstrated the confidence of CPRCMs in estimating snowfall and snowpack

68   in the central U.S. Furthermore, the importance of CPRCMs in representing dry spell, dry and wet extremes induced

69   by local convective activity across Africa has also been found in Kendon et al. (2019), Chapman et al. (2023) further

70   confirmed its benefit in capturing rare rainfall extreme and local feature. In UK, Kendon et al. (2023) and Kent et al.

71   (2022) have found the benefit of CPRCMs compared to RCMs with convection parameterization schemes.

72   Additionally, the superior performance in capturing hourly and daily extreme precipitation including return-level,

73   frequency and intensity from CPRCMs over Alpine in Europe, has also been highlighted by Adinolfi et al. (2021),

74   Dallan et al. (2023) and Giordani et al. (2023).

75   Northern Europe has been reported to experience the most increase in precipitation, as indicated by Dyrrdal et

76   al., (2023), where a novel CPRCMs have been developed within the Nordic Convection Permitting Climate

77   Projections project (NorCP) based on the convection-permitting HARMONIE-Climate model (HCLIM), cycle 38

78   (HCLIM38) at a resolution of 3 km (HCLIM38-AROME) and 12km (HCLIM38-ALADIN). For convenience,

79   HCLIM3 and HCLIM12 are used in the following to represent the regional climate models HCLIM38-AROME and

80   HCLIM38-ALADIN, respectively. HCLIMs also indicate both HCLIM3 and HCLIM12. Through comparisons of

81   seasonal precipitation, daily mean precipitation, higher-intensity daily precipitation, the diurnal of hourly

82   precipitation including frequency and intensity from HCLIM3 and HCLIM12 over Fenno-Scandinavia, Lind et al.

83   (2020) emphasized the add-value of CPRCMs in reproducing extreme precipitation, primarily over complex terrain,

84   compared to a coarser-scale model. Médus et al. (2022) also noted that the summer diurnal cycle of frequency and

85   intensity of hourly precipitation was correctly captured in HCLIM3 compared to HCLIM12 in the Nordic region,

86   with HCLIM12 underestimating the diurnal cycle. However, the evaluation and conclusions from Lind et al. (2020)

87   and Médus et al. (2022) mainly focused on the large regional and country scale of Fenno-Scandinavia, overlooking

88   the added values of CPRCMs at local scale. Furthermore, Thomassen et al. (2023) observed that HCLIM3 tends to

89   exhibit underestimations in monthly precipitation and a later evening peak compared to sub-kilometre models. They

90   found that the advantages of sub-kilometer models were not outstanding. These evaluations were based on gridded

91   datasets, which introduce uncertainty at the local scale, especially over complex orography (Lussana et al., 2019).

92   As Chapman et al. (2023) demonstrated, who underscored the importance of assessing rare extreme rainfall events

93   in eastern African using convection-permitting models and parameterization convection models at both grid and

94   station scales, that the extreme from grids representing rainfall averaged over a larger area are damped and hence the

95   return-level will be smaller than observation. They found that the station-derived shape parameters and return levels

96   are aligned with observations and suggested the significance of site-specific analysis and evaluations. The error

97   induced by station density in gridded dataset has also been indicated in Gervais et al. (2014b), who suggested the

98   source of large errors in gridded dataset when station density is low. Consequently, a comprehensive evaluation and

99   analysis of the added value from CPRCMs compared with RCMs that incorporates both regional and local scales is

100   crucial for extreme precipitations.

101   We acknowledge that Norway, a Nordic country, is representative of diverse climate features due to its

102   extended latitude, rugged coastline, plateaus, and complex orography. The dominances of precipitation between the

103   coastal and inland regions over Norway are distinctly different, and most of studies focusing on the hydrology and

104 meteorology over Norway were based on the divided regions (Vormoor et al., 2016; Poujol et al., 2021; Konstali

105 and Sorteberg, 2022). By dividing region with its characteristics, a more thorough comprehension of add-value of

106 CPRCMs in capturing extreme precipitation can be reached. Therefore, reliable evaluation about analyzing the add-

107 value of CPRCMs in capturing extreme precipitation should be scaled to region or local scale.

108   In the complex mountain areas, extreme precipitation is triggered by the interaction of large-scale atmospheric

109 activity and local orography property, which may cause severe hydrometeorological hazards, such as flash flooding.

110 However, understanding the orographic impact in precipitation in complex orography is challenging due to sparse

111 observations (Rossi et al., 2020). The poor representation of RCMs in capturing local precipitation have been

112 indicated in Knist et al. (2020). Importantly, CPRCMs shows advantage in reproducing precipitation bias over

113 higher complex orography in the Alpine, as shown in Lind et al. (2016) and Reder at al. (2020). Furthermore, the

114 better representation of sub-daily and daily heavy precipitation from CPRCMs over the Alpine have also been found

115 in Ban et al. (2020) and Dallan et al. (2023). Marra et al. (2021) and Dallan et al. (2023) also confirmed the

116 efficiency of CPRCMs in reproducing the reverse orography effect on hourly extreme precipitation. The relationship

117 between extreme precipitation and elevation may vary depending on latitude and climate zones (Amponsah et al.,

118 2022). Rossi et al. (2020) and Mahoney et al. (2015) found the weak depend of subdaily precipitation on elevation in

119 the Colorado, USA. Opposing the orographic enhance on daily precipitation, Dallan et al. (2023) indicated the no

120 evident relation of daily precipitation on elevation. It is worth noting that the potential added value of CPRCMs in

121 representing orographic effects compared to RCMs has not been explored. Moreover, the performance of CPRCMs

122 varies with seasons, which underscores the need to explore the orographic effects on seasonal extremes. Thus, we

123 fill this knowledge gap by characterizing orographic impact on hourly and daily extreme precipitation seasonally.

124   As highlighted by Konstali and Sorteberg (2022), there can be significant uncertainties associated with the

125 interpolation of grided precipitation data. Besides, the benefit for precipitation spatial evaluation based on in-situ

126 observation has also been reported in Thomassen et al. (2023). Therefore, the evaluation of extreme precipitation

127 from HCLIM3 and HCLIM12 here, is based on both gridded precipitation and in-situ observation. Our study aims to

128 address the value of CPRCMs (HCLIM3) in capturing the characteristics of extreme precipitation in Norway,

129 comparing it with a coarser resolution model (HCLIM12) as well as both of the in-situ and gridded precipitation

130 observations. Here, our contribution to the existing literature, e.g., Médus et al. (2022), revolves around the added

131 value of CPRCMs in the extreme precipitation characteristics, encompassing a range of metrics.

132   The main objectives of this study are to: (1) enhance the understanding of convection-permitting climate

133 models and highlighting the added value of CPRCMs by comparing their effectiveness in simulating extreme

134 precipitation with that of regional climate models from regional to local scales; (2) assess HCLIM3's capability in

135 depicting orographic effects on seasonal extreme precipitation. This research explores whether the benefits provided

136 by CPRCMs are consistent in different regions driven by varying physical processes for precipitation. Finally, our

137 study delves into the analysis of the intensity and frequency of extreme precipitation events, offering insights into

138 local and regional variations.
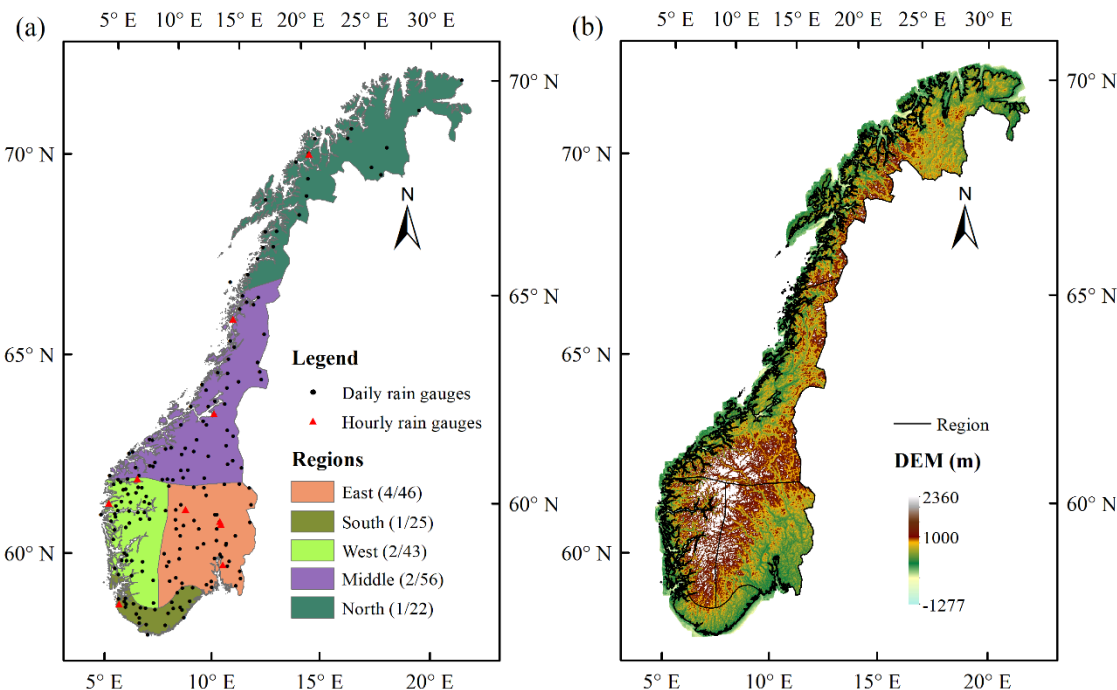
2 Study area and data

2.1 Study area

Figure 1: (a) The division of five regions in Norway. In the legend, the numbers shown in the brackets after each region represent the available size of hourly / daily stations in the region during 1999 – 2018. For example, East (4/46) means that there are available data from 4 hourly stations and 46 daily stations in the East during 1999-2018; (b) Spatial distribution of topography over Norway.

The different climate regimes between coastal and inland regions over Norway compels the analysis of hydro-meteorology based on divided regions. Based on similar seasonal cycle characteristics, Michel et al. (2021) and Konstali and Sorteberg (2022) divided the Norwegian continent into eight regions. Taking into account the spatial distribution of rain gauges and ensuring that each region has at least one hourly rain-gauge, we combined the south and southwest into the south, and the middle-inland and north into the north. Therefore, mainland Norway in this study is divided into five regions: East (E), South (S), West (W), Middle (M), and North (N), as shown in Fig. 1.

The study areas cover the mainland Norway which has unique climate characteristics within different regions. Precipitation in Norway primarily occurs along the coast in late autumn and winter, while inland areas receive more precipitation in summer. The eastern region with stratiform precipitation originating from south is dominant by continental climate, with convective precipitation in summer. The west coast of Norway is strongly affected by the North Atlantic storm track, where precipitation from frontal systems and landfalling storms is enhanced due to the orographic uplift over Scandinavia (Poujol et al., 2021). Most extreme events occurring in the western region with abrupt topography, are mainly related to atmospheric rivers (AR), which are generally linked to extratropical cyclones during cooler seasons (Whan et al., 2020). Additionally, in the summer, AR coincides with more frequent convective activities (Poujol et al., 2021). The southern region lies at the end of the climatological jet and is

163 regularly affected by the AR especially during the Zonal and Atlantic trough weather regimes (Michel et al., 2021),

164 while convective activities play a crucial role in the southern regions in summer (Li et al., 2020b). For the middle

165 and northern regions, 59% of extremes are associated with AR, and the precipitation rate decreases moving inland

166 (Konstali and Sorteberg, 2022).

167 **2.2 Data**

168 We utilize the outputs of double nested model simulations from the HCLIM38 model, which include different

169 configuration settings for each spatial resolution: HCLIM3 and HCLIM12. HCLIM12 covers most of Europe with

170 313 ×349 grid-points using the ERA-Interim reanalysis (~80 km) as the boundary condition, and HCLIM3 spans the

171 Fenno-Scandinavia region with 637×853 grid-points using the output of the HCLIM12 as the boundary condition for

172 every 3 h. Importantly, the convection-parameterization scheme was switched-off in HCLIM3, allowing for an

173 explicit representation of convection processes. The present-day simulations from HCLIM3 and HCLIM12 span the

174 years 1997-2018. For more comprehensive information, refer to the work of Lind et al. (2020) and Médus et al.

175 (2022).

176   This study primarily focuses on assessing the performance of HCLIM3 and HCLIM12 in simulating hourly

177 and daily extreme precipitation events in mainland Norway for the present-day period (1997-2018, with the first two

178 years excluded). The model outputs from HCLIM3 and HCLIM12 are specifically extracted for mainland Norway.

179 Before analysis, HCLIM3 data was remapped to the HCLIM12 grid (12km) using a bilinear interpolation method.

180   Precipitation from the seNorge2018 (SeNorge) gridded dataset, covering Norway with 1-day temporal and 1

181 km spatial resolution since 1957 (Lussana et al., 2019), is used as the observation dataset to evaluate the

182 performance of HCLIM3 and HCLIM12 during 1999-2018. Precipitation from the SeNorge2 gridded dataset, with

183 1-hour temporal and 1 km spatial resolution, is also applied to evaluate the hourly result during 2010-2018 (Lussana

184 et al., 2018). In addition, in-situ precipitation of observations, including both 1-hour and 1-day resolutions, are

185 downloaded from Norwegian Meteorological Institute <u>Frost API (met.no)</u>.

186 **3 Methods**

187 **3.1 Evaluation of precipitation**

188 To evaluate the characteristics of precipitation extremes between HCLIM3 and HCLIM12, we compared the

189 historical simulations with daily SeNorge gridded dataset, hourly SeNorge2 gridded dataset and in-situ observations.

190 We only keep the stations that have less than 10% of the data missing during 1999-2018 and consider station

191 distribution uniformity, which give a total of 192 daily stations and 10 hourly stations, respectively, over Norway

192 (Fig. 1, Table S1 and Table S2). In this study, the evaluation based on in-situ observation and gridded dataset

193 (SeNorge and SeNorge2) was defined as the local scale and regional scale, respectively.

194   Remapping finer-resolution data to a coarser resolution reduces the influence of such artifacts by averaging out

195 the variability. This approach is consistent with the methodology used by Lind et al. (2020) and Médus et al. (2022),

196 who also remapped all data to a coarser grid when comparing the performance of HCLIM3 and HCLIM12. Lind et

197   al. (2020) observed that the differences between HCLIM3 data remapped to the coarser native grid of HCLIM3 and
198   the HCLIM12 grid were minimal. Importantly, they found that the improvements of HCLIM3 persisted even after
199   spatial aggregation, indicating that the enhanced resolution of the model offered benefits that were preserved when
200   viewed on a coarser grid. Therefore, HCLIM3, SeNorge and SeNorge2 were remapped to HCLIM12 grid~12 km for
201   the evaluation at regional scale. For the SeNorge and SeNorge2 based assessments, the extreme indices are first
202   calculated at the grid-point level and then the regional averages are computed. For the evaluation based on in-situ
203   observation, HCLIM3 and HCLIM12 were interpolated to the 192 daily rain-gauges and 10 hourly rain-gauges to
204   calculate the indices using bilinear interpolation method.

205   For the evaluation of extreme precipitation, we examined the maximum 1-day precipitation (Rx1d), maximum
206   1-hour precipitation (Rx1h), return-period-based precipitation amounts at 5, 10, 20, and 50-year return periods, and
207   seasonality of frequency/intensity from regional to local scales. The calculation of seasonal Rx1d/Rx1h was based
208   on the maximum value within one season per year.

209   **3.2 Extreme precipitation indices**

210   The Generalized Extreme Value (GEV) distribution was used to estimate precipitation intensity for specific return
211   periods (e.g., 5, 10, 20, and 50 years). The return levels were calculated by fitting the annual maximum discharge
212   derived from observed and simulated daily data (both gridded and rain gauges), and hourly data (only 10 rain
213   gauges), to GEV distribution. Then, the quantile Z_p of the GEV distribution with a return period of $\frac{1}{p}$ can be
214   obtained. GEV distribution has been widely used to model extreme events in meteorology (Coles et al., 2003). The
215   cumulative distribution function $F(x)$ and probability density function $f(x)$ of GEV were as follows to calculate the
216   return level Z_p:

217

218    $$F(x) = exp\left\{-\left[1 - k\left(\frac{x-\xi}{\alpha}\right)\right]^{1/k}\right\}, k \neq 0 \qquad (1)$$

219    $$f(x) = \frac{1}{\alpha}\left[1 - k\left(\frac{x-\xi}{\alpha}\right)\right]^{1/k-1} exp\left\{-\left[1 - k\left(\frac{x-\xi}{\alpha}\right)\right]^{1/k}\right\} \qquad (2)$$

220    $$Z_p = \xi - \frac{\alpha}{k}\{1 - [-log(1-p)]^{-k}\} \qquad (3)$$

221

222   Where, α, ξ, and k indicates the scale, location and shape parameter, respectively. Kolmogorov-Smirnovs,
223   Anderson-Darlings, and Chi-Square tests were performed to determine if the GEV was accepted to fit the maxima
224   series.

225

226   **3.3 Quantification of the orographic effect**

227   The orographic effect on Rx1h and Rx1d precipitation was explored by looking at the relationship with elevation of
228   the annual and seasonal maxima from regional to local scales. A linear regression model (Di Piazza et al., 2011) was
229   utilized to approximate the relations. The relationship of elevation with observation (Rx1h: SeNorge2; Rx1d:
230   SeNorge and daily in-situ observation) and simulation (HCLIM3 and HCLIM12) was fitted to compute the linear

231   regression slope. To eliminate the impact of unit (Rx1h and Rx1d), the slope is transferred to relative slope with

232   respect to the average value of extreme precipitation, expressed as percentage precipitation (%) per kilometer of

233   elevation. The orographic effect at local scale was only based on daily in-situ observation due to the limited hourly

234   in-situ observation. At local scale, the elevation for each rain-gauges was extracted according to the digital elevation

235   model. At regional scale, the grid of digital elevation model and HCLIM3 was resample to the same grid resolution

236   of 12 km as HCLIM12 before calculation. Only the grids and stations above sea level of 0 m are included to

237   quantify the orographic effect.

238   If the precipitation increases with elevation, it means that the orographic effect on extreme precipitation; if the

239   precipitation decreases with elevation, its means that the reverse orographic effect on extreme precipitation.

240   **4 Results**

241   **4.1 Evaluation of daily extreme with SeNorge**

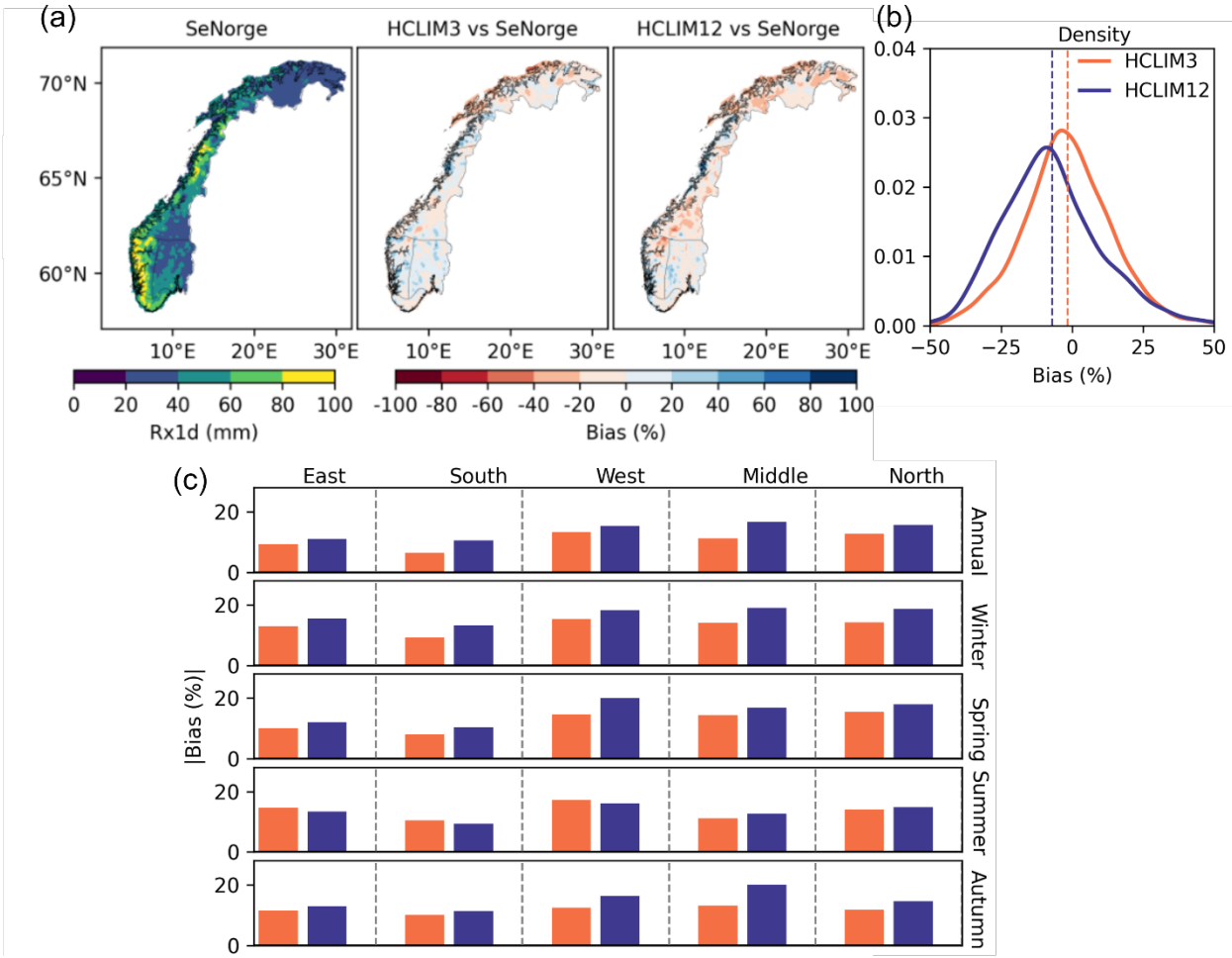242   **4.1.1 Maximum 1-day precipitation (Rx1d)**

243

Figure 2: (a) The annual Rx1d of SeNorge, and the percentage bias of Rx1d from HCLIM3 and HCLIM12 to SeNorge during 1999-2018; (b) density plot of the percentage bias distribution for annual Rx1d from HCLIM3 and HCLIM12 compared to SeNorge for Rx1d during 1999-2018 (The dashed lines represent the mean bias); (c) the absolute percentage bias of annual and seasonal Rx1d from HCLIM3 and HCLIM12 to SeNorge for five regions. The bias is first calculated at the grid-point level, and then regional averages are computed. For (a) and (b), the percentage bias is equal to model simulations minus observations, divided by observations. For (c), the absolute percentage bias is calculated as the absolute difference between simulations and observations, divided by observations.

Figure 2 provides a comprehensive comparison of percentage biases of Rx1d from HCLIM3 and HCLMI12 compared to SeNorge. From Fig. 2 (a), we can see that HCLIM12 has more grids with underestimated Rx1d than HCLMI3 in Norway, which is confirmed clearly in Fig. 2 (b) showing density plot of the percentage bias distribution from two models compared with SeNorge. Specifically, more grids from HCLIM3 than HCLIM12 tend to overestimate Rx1d within the 0-25 % range, while HCLIM12 leans towards larger underestimation within the -10-50%. The density curve in Fig. 2 (b) reflects a higher peak at 0 for HCLIM3, indicating a more accurate representation of Rx1d with an average dry-bias with 1.6%. Conversely, HCLIM12 shows a 7% dry-bias for Rx1d on average.

 Figure 2 (c) shows the absolute percentage bias of annual and seasonal Rx1d from HCLIM3 and HCLIM12 compared to SeNorge for five regions in four seasons. In annual, HCLIM3 exhibit added value in capturing annual Rx1h in the five regions compared to HCLIM12. HCLIM3 better captures Rx1d in four seasons and annual for five regions than HCLIM12, while HCLIM12 shows larger bias in most regions except in the east, south and west during summer. In summer, HCLIM3 only outperforms Rx1d in the middle and north over HCLIM12. Overall, HCLIM3 shows notably added value in Rx1d comparing with HCLMI12 across regions and seasons except in summer.

 Furthermore, as shown in Fig. 3, a comparison of the Rx1h percentage biases of HCLIM3 and HCLIM12 with SeNorge2 for the period 2010-2018 demonstrates that HCLIM3 has a clearly added value in simulating the annual Rx1h in Norway, with smaller wet biases on average, while HCLIM12 shows larger dry biases over the whole of mainland Norway. At the regional scale, HCLIM3 also shows added value in capturing annual and seasonal Rx1h than HCLIM12 in five regions except west and middle regions. Specifically, in the west region, HCLIM3 exhibits larger absolute percentage biases than HCLIM12 in annual Rx1h and seasonal Rx1h than HCLIM12, except in spring. In summer, only in the south and north regions, the Rx1h bias of HCLIM3 is smaller than that of HCLIM12.
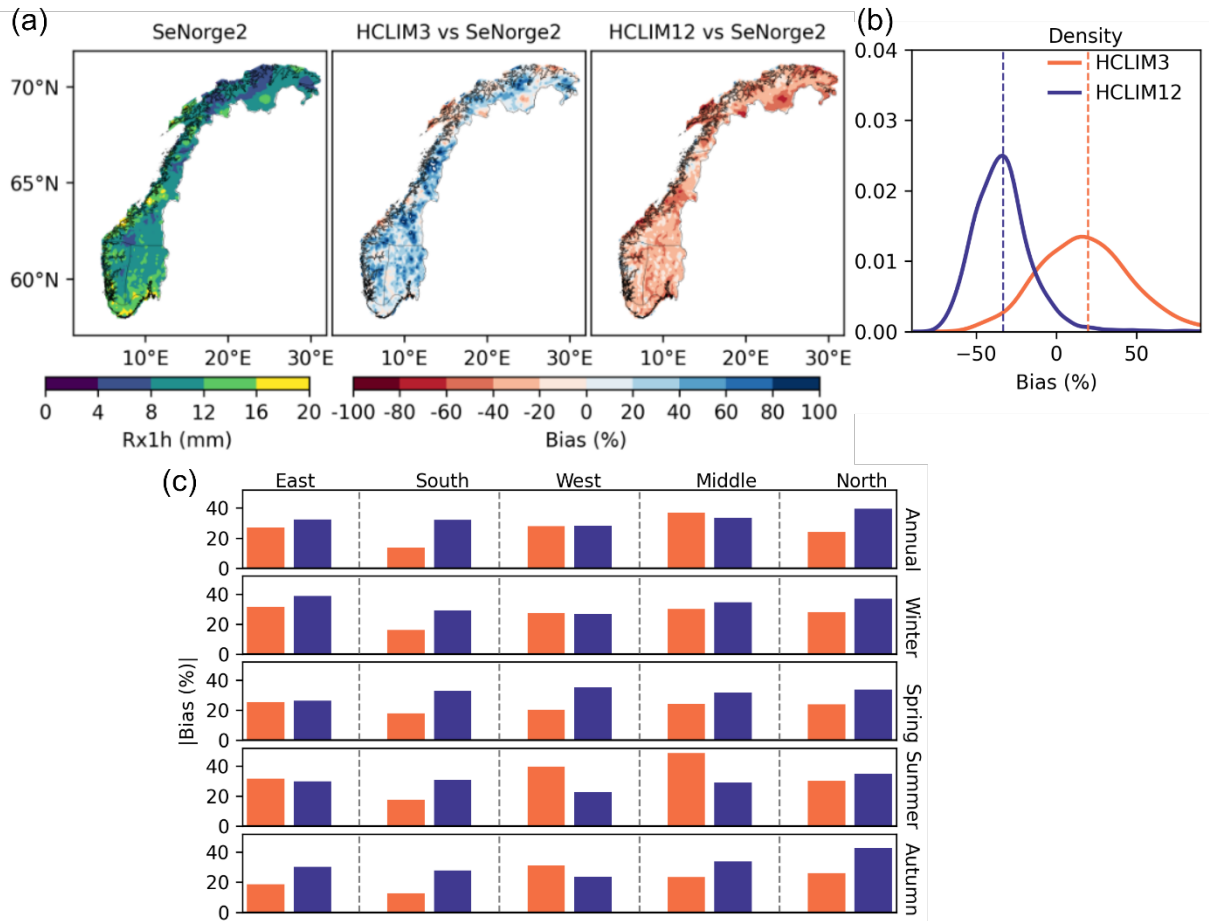
Figure 3: (a) The annual Rx1h of SeNorge2, and the percentage bias of Rx1h from HCLIM3 and HCLIM12 to SeNorge2 during 2010-2018; (b) density plot of percentage bias for annual Rx1h distribution from HCLIM3 and HCLIM12 compared to SeNorge2 during 2010-2018 (The dashed lines represent the mean bias); (c) the absolute percentage bias of seasonal Rx1h from HCLIM3 and HCLIM12 to SeNorge2 for five regions. For (a) and (b), the percentage bias is equal to model simulations minus observations, divided by observations. For (c), the absolute percentage bias is calculated as the absolute difference between simulations and observations, divided by observations.

4.1.2 Return levels

Figure 4 shows the bias in estimated daily precipitation for 5-, 10-, 20-, and 50-year return periods during 1999-2018 across five regions (compared to SeNorge). The great interregional variation is shown between HCLIM3 and HCLIM12. Relative to SeNorge, HCLIM3 tends to overestimate return-levels in the eastern and western regions, while underestimates them in the others. By comparison, except for the east region where HCLIM12 shows overestimation, the extreme precipitation estimates in most other regions are underestimated. The performance of HCLIM3 in capturing extremes varies across regions. HCLIM3 and HCLIM12 exhibit percentage biases of opposite sign in simulating return level precipitation in the western region, where HCLIM3 overestimates and HCLIM12 underestimates precipitation at different return periods. In the western, middle, and northern regions, HCLIM3 outperforms HCLIM12 in all return periods, but the performance is less satisfactory in the eastern region.

291   Given the societal impacts of precipitation extremes, understanding how HCLIM3 and HCLIM12 represent

292   these extremes is crucial. The physical processes driving precipitation in inland and coastal regions, as highlighted

293   by Konstali and Sorteberg (2022), emphasize the need for a separate evaluation for each region with different

294   characteristics. This approach ensures a more robust assessment, providing valuable information for regional
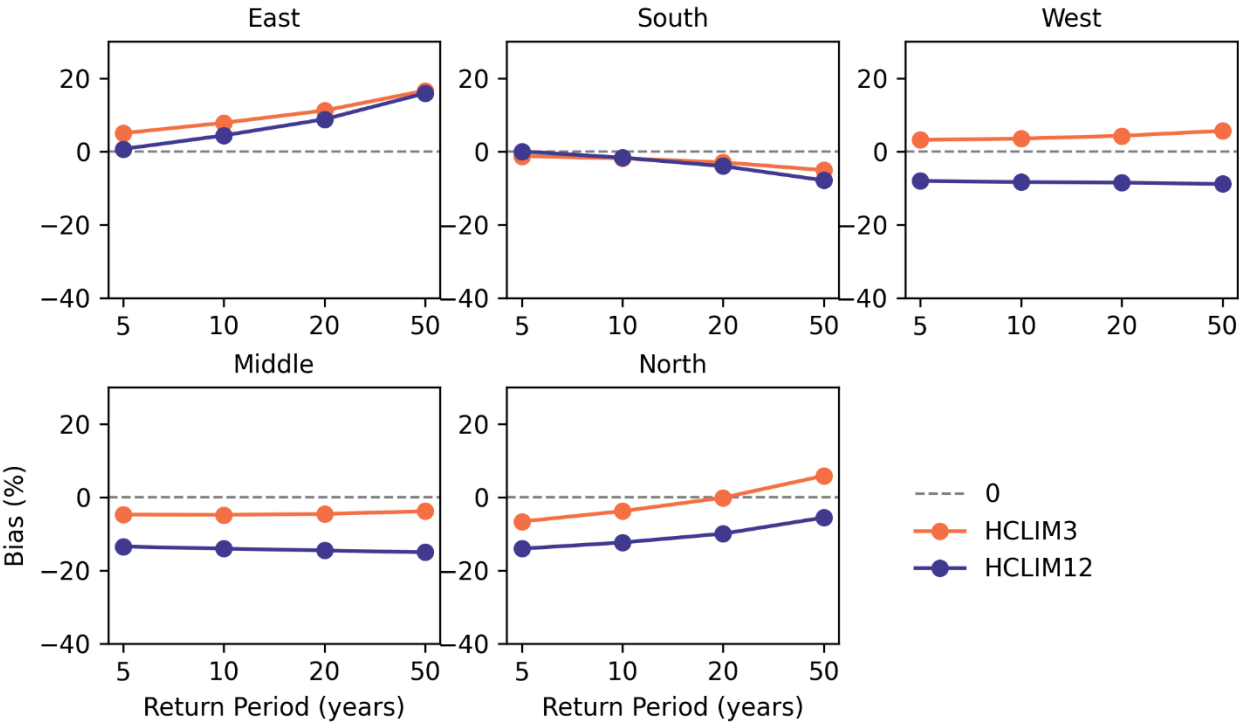
295   authorities.

296

297   **Figure 4: Percentage bias of extreme daily precipitation exceeding the 5-year to 50-year return periods over five regions**

298   **between SeNorge and HCLIMs (i.e., HCLIM3 and HCLIM12). Return periods of 5-, 10-, 20-, and 50-year are calculated**

299   **on the basis of GEV.**

4.2 Evaluation of daily extreme with in-situ data

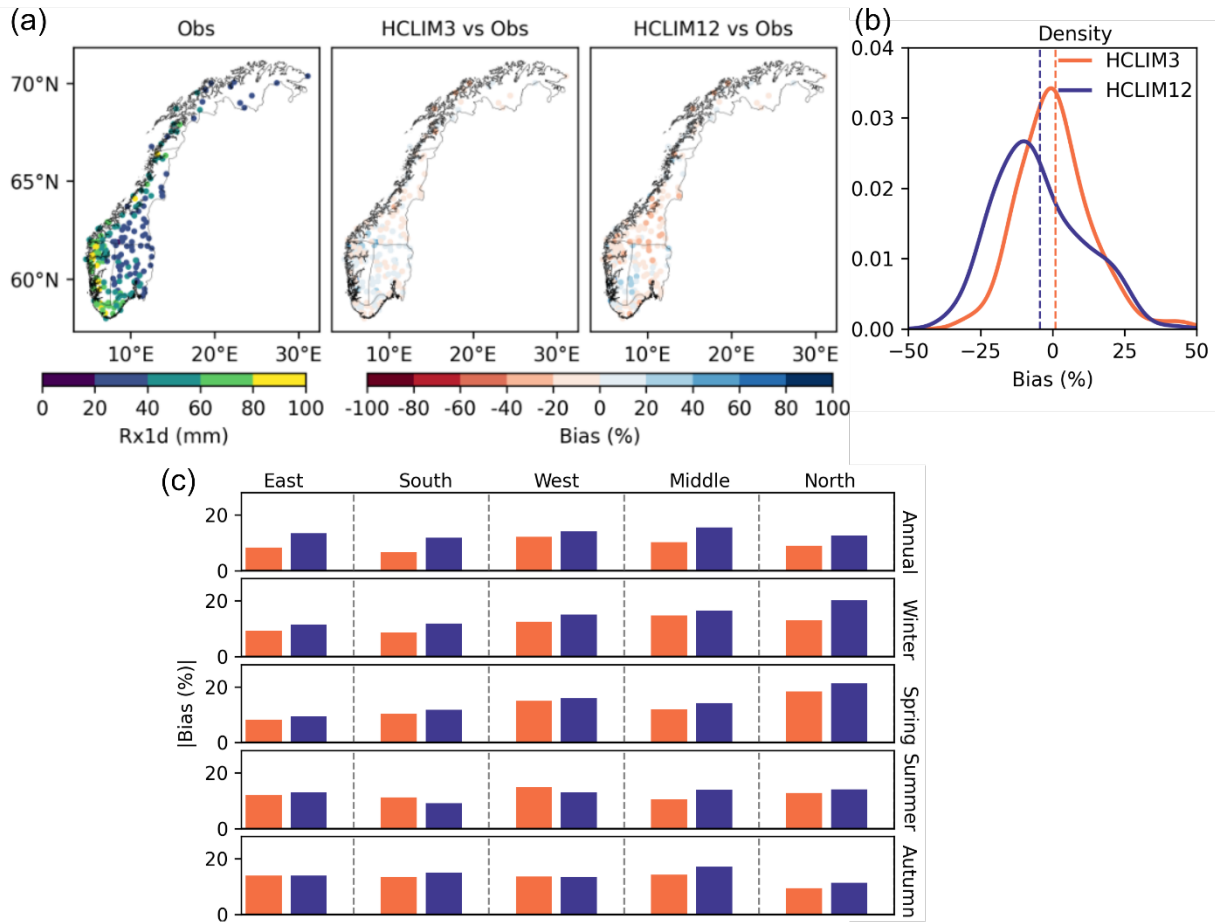### 4.2.1 Maximum 1-day precipitation (Rx1d)

Figure 5: (a) The annual Rx1d of in-situ observation, and the percentage bias of Rx1d from HCLIM3 and HCLIM12 to in-situ observation during 1999-2018 over 194 stations; (b) density distribution of percentage bias for annual Rx1d between HCLIMs and observations from 194 stations during 1999-2018 (The dashed lines represent the mean bias); (c) the absolute percentage bias of seasonal Rx1d between HCLIMs and observations across the five regions. For (a) and (b), the percentage bias is equal to model simulations minus observations, divided by observations. For (c), the absolute percentage bias is calculated as the absolute difference between simulations and observations, divided by observations.

Similar to the regional results in Fig. 2, Fig. 5 shows the percentage bias of annual and seasonal Rx1d from HCLIM3 and HCLIM12 in comparison to in-situ observations. Notably, a difference between HCLIM3 and HCLIM12 can be seen at local scale compared to regional result: a greater number of sites from HCLIM3 approach zero-bias, and more grids from HCLIM12 shows a dry bias about 10-40%, as shown in Fig. 5 (b). On average, HCLIM12 with 4.5% dry-bias tends to underestimate annual Rx1d, while HCLIM3 represents added value in capturing annual Rx1d with 1% wet-bias on average at local scale. Furthermore, HCLIM3 shows added value in simulating the annual Rx1h at local scale in all regions.

From a seasonal perspective, as shown in Fig. 5 (c), overall, HCLIM3 shows added value in capturing the seasonal Rx1d in most regions and seasons, except for summer. Specifically, HCLIM3 performs better than

319   HCLIM12, except for the western and southern region, where HCLIM3 exhibits a larger bias in summer Rx1d. In

320   particular, the added value of HCLIM3 in simulating autumn Rx1d in the east and west is not as obvious when

321   compared to HCLIM12.

322   It is noteworthy that at the local scale, HCLIM3 and HCLIM12 perform similarly to the regional results in most

323   regions. There are some exceptions, such as, HCLIM3 shows larger biases in summer Rx1d in the south and west

324   compared with HCLIM12 at both regional and local scales. In contrast to the clearly larger bias in Rx1h at the

325   regional scale for both HCLIM3 and HCLIM12, a relatively smaller bias in Rx1d is demonstrated at both regional

326   and local scales. At the regional scale, HCLIM3 exhibits added value in all seasons except summer, while at the

327   local scale, HCLIM3 and HCLIM12 show similar biases in autumn Rx1d in the east and west, which means that the

328   advantage of HCLIM3 over HCLIM12 at the local scale in autumn weakens in the west and east compared with the

329   regional scale.

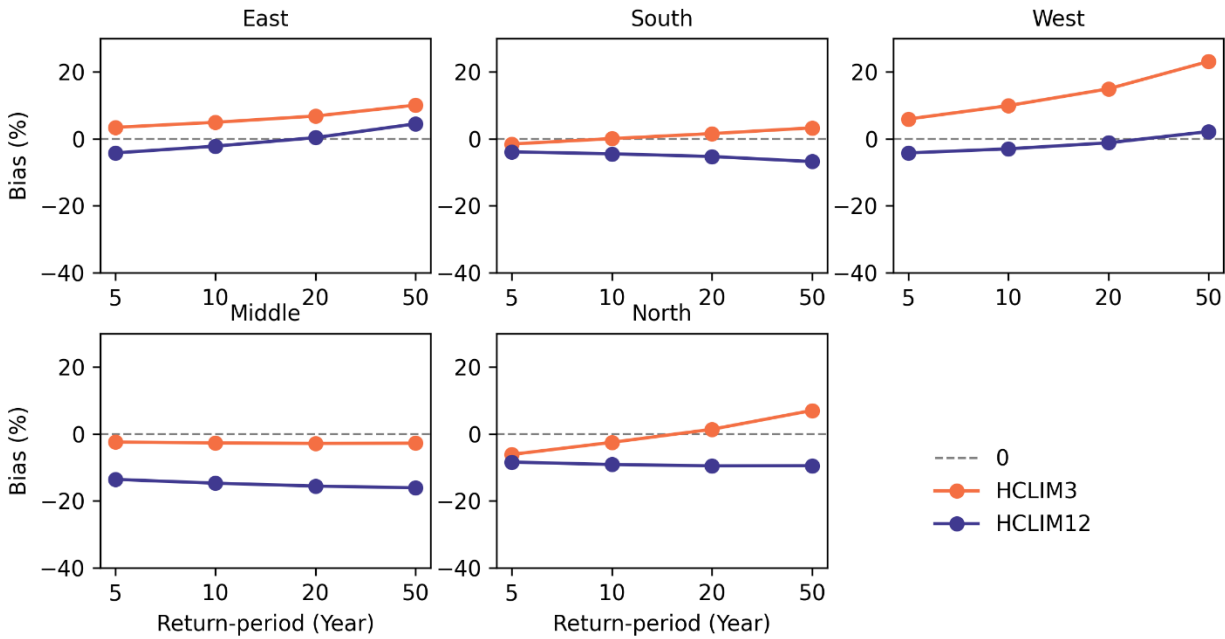330   **4.2.2 Return-levels**

331

332   **Figure 6: Percentage bias of extreme daily precipitation exceeding the 5-year to 50-year return periods over five regions**
333   **between HCLIMs (i.e., HCLIM3 and HCLIM12) and in-situ observation in the 192 daily rain-gauges. Return periods of**
334   **5-, 10-, 20-, and 50-year are calculated on the basis of station-scale GEV.**

335

336   Figure 6 shows the percentage bias of the estimated daily return levels (e.g., 5-, 10-, 20-, and 50-year return periods)

337   from HCLIM3 and HCLIM12 compared to observations for the period 1999-2018. The figure illustrates the average

338   bias of return-levels for the stations in the corresponding regions. Compared with the in-situ observation, HCLIM3

339   overestimates the return levels in the east and west for all return periods (5-, 10-, 20-, and 50-year) and

340   underestimates return levels in the south and north for 20- and 5-year return periods, while HCLIM12

341   underestimates the return levels in all regions. Generally, HCLIM3 can more accurately represent the return levels in

342   most regions compared to HCLIM12. The biases of HCLIM3 and HCLIM12 vary across regions and return periods.

343   HCLIM3 has lower biases than HCLIM12 in most regions, except for the eastern and western regions. Both

344   HCLIM3 and HCLIM12 perform well in the southern region. In addition, Fig. S1 shows the range of the return

345   levels for all stations in the corresponding region, and HCLIM3 introduces larger variations in the western and

346   southern regions compared with HCLIM12, as indicated by the wider whiskers.

347   **4.3 Evaluation of hourly extreme with in-situ data**

348   **4.3.1 Maximum 1-hour precipitation (Rx1h)**

349   The time evolution of annual Rx1h from HCLIM3 and HCLIM12 is compared to in-situ observation during 1999-

350   2018, as shown in Fig. 7. Compared to HCLIM12, HCLIM3 shows distinct superior in capturing the time evolution

351   of annual Rx1h, even with underestimation and time shifting at some local places. For example, the annual Rx1h

352   above 25 mm/hour at Kvithamar (SN69150), Særheim (SN44300), Tromsø - Holt (SN90400), Tjøtta (SN76530) and

353   Løken i Volbu (SN23500) is struggle to be captured by HCLIM3 and HCLIM12. However, HCLIM3 well capture

354   the annual Rx1h in other local places, despite of the time deviation of annual Rx1h. Taking the site Østre Toten -

355   Apelsvoll (SN11500) as an example to illustrate the time deviation: HCLIM3 simulate that the annual Rx1h (37

356   mm) in the past 20 years was in 2001, four years earlier than the in-situ observation (35 mm). Furthermore, to better

357   assess the annual variability of Rx1h, we extracted grids within a 12 km radius of each station and calculate the

358   uncertainty range (Fig. S2), which reveals that the interpolated local Rx1h precipitation from HCLIM12, particularly

359   over grids with a larger area, tends to be damped, resulting in a narrower range than HCLIM3. Based on station

360   statistics of annual mean Rx1h for ten stations in Norway, the boxplot (Fig. 7) shows that the annual mean Rx1h of

361   HCLIM3 is within the range of observed values. In contrast, HCLIM12 consistently underestimates Rx1h, with all

362   its values being below the observed minimum. Despite outperforming than HCLIM12, it is noteworthy that

363   HCLIM3 demonstrates limitations in reproducing the accurate occurrence time and magnitude of annual Rx1h at

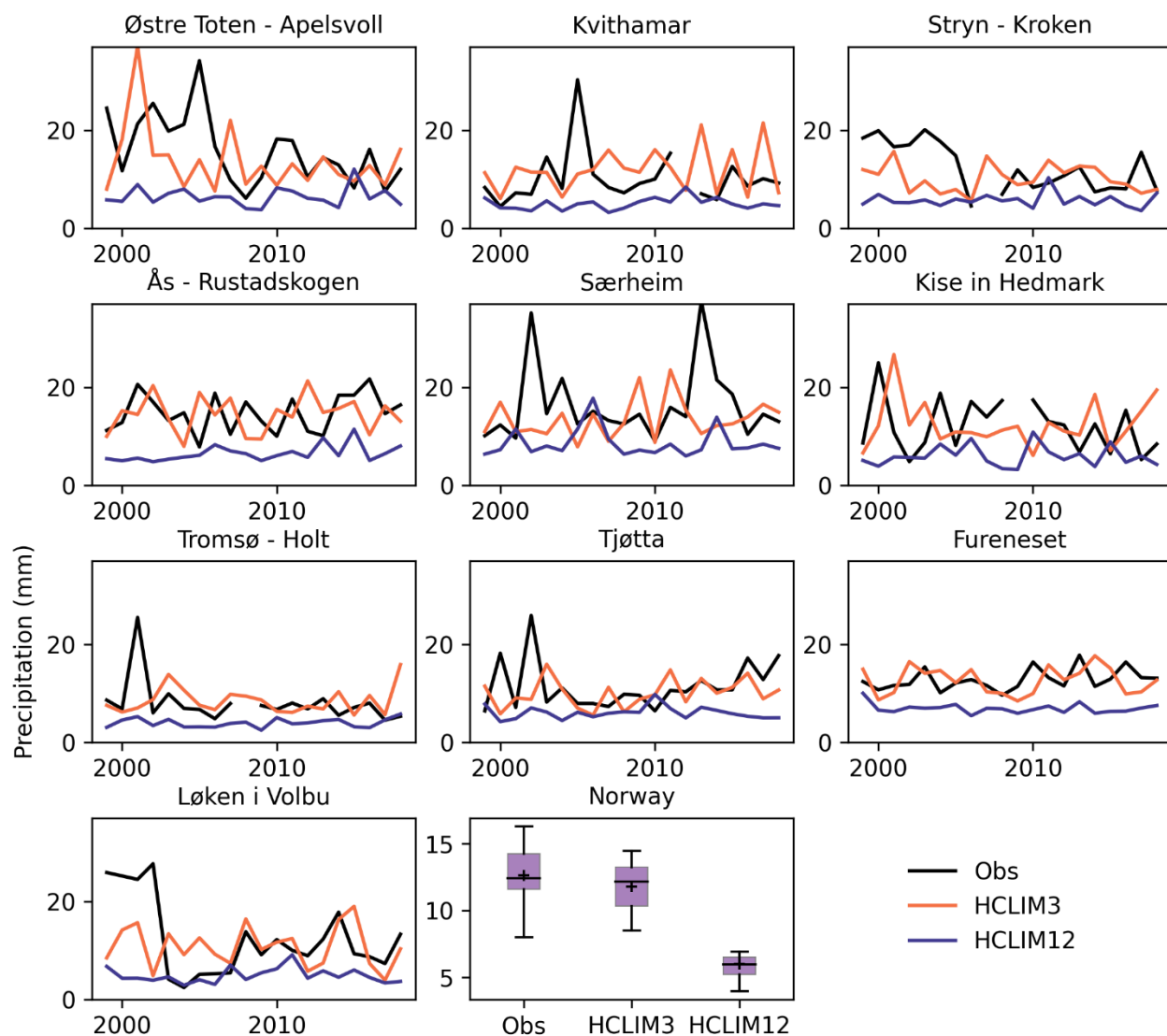364   local-level in Norway.

365

Figure 7: Time evolution of Rx1h precipitation for each year from observation, HCLIM3 and HCLIM12 during 1999-2018 at 10 rain-gauges (Table S1).
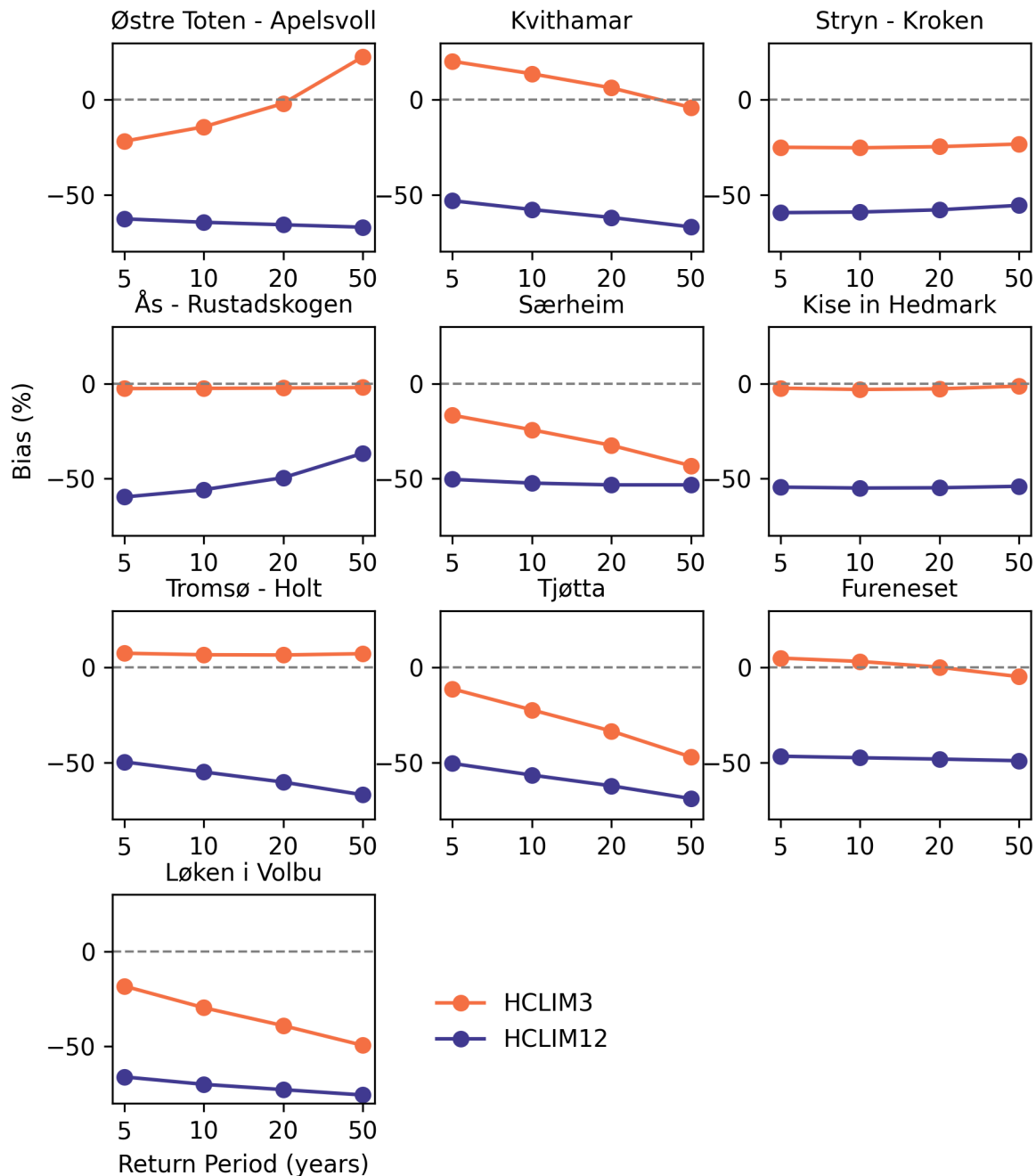
4.3.2 Return levels

Figure 8: Percentage bias of extreme hourly precipitation exceeding the 5-year to 50-year return periods between HCLIMs (i.e., HCLIM3 and HCLIM12) and in-situ observation in the 10 hourly rain-gauges. Return periods of 5-, 10-, 20-, and 50-year are calculated on the basis of station-scale GEV.

At the local and hourly scale, HCLIM3 has a better representation of hourly extreme events at the 5-, 10-, 20-, and 50-year return periods compared to HCLIM12. Although both HCLIM3 and HCLIM12 tend to underestimate the annual Rx1h for all return periods at almost stations (Fig. 8), the biases between the observations and the

380 interpolated HCLIM3 for all ten rain gauges are consistently lower than those of HCLIM12 for all return periods.
381 The exceptions are Kvithamar (SN69150), Tromsø - Holt (SN90400) and Fureneset (SN56420) which present at all
382 return periods, and Østre Toten - Apelsvoll (SN11500) which present at a 50-year return period, where HCLIM3
383 slightly overestimation. Notably, the return levels of hourly extreme events at all ten sites are accurately captured by
384 HCLIM3, demonstrating its better ability to capture the extreme hourly precipitation at the 5-, 10-, 20-, and 50-year
385 return periods in localized areas, compared to HCLIM12. This result underscores the added value of CPRCMs in
386 representing hourly extreme precipitation at a very localized scale, despite the overall underestimation of return
387 levels by both HCLIM3 and HCLIM12.
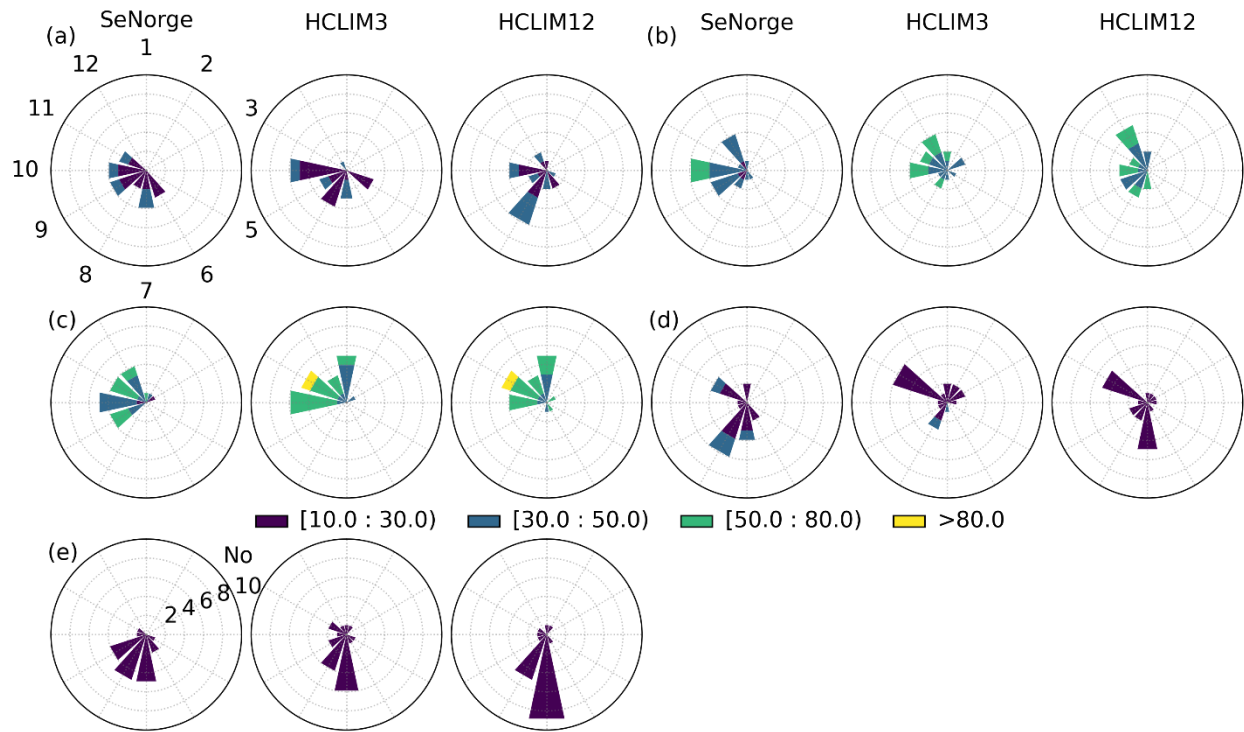
388 **4.4 Evaluation of seasonality**

389
390 **Figure 9: The seasonality of frequency and magnitude of Rx1d precipitation from the SeNorge, HCLIM3 and HCLIM12**
391 **during 1999-2018 over different regions: a) Eastern, b) South, c) West, d) Middle, f) North. The color represents the**
392 **magnitude of Rx1d (m³/s). Winter: December, January, February; Spring: March, April, May; Summer: June, July,**
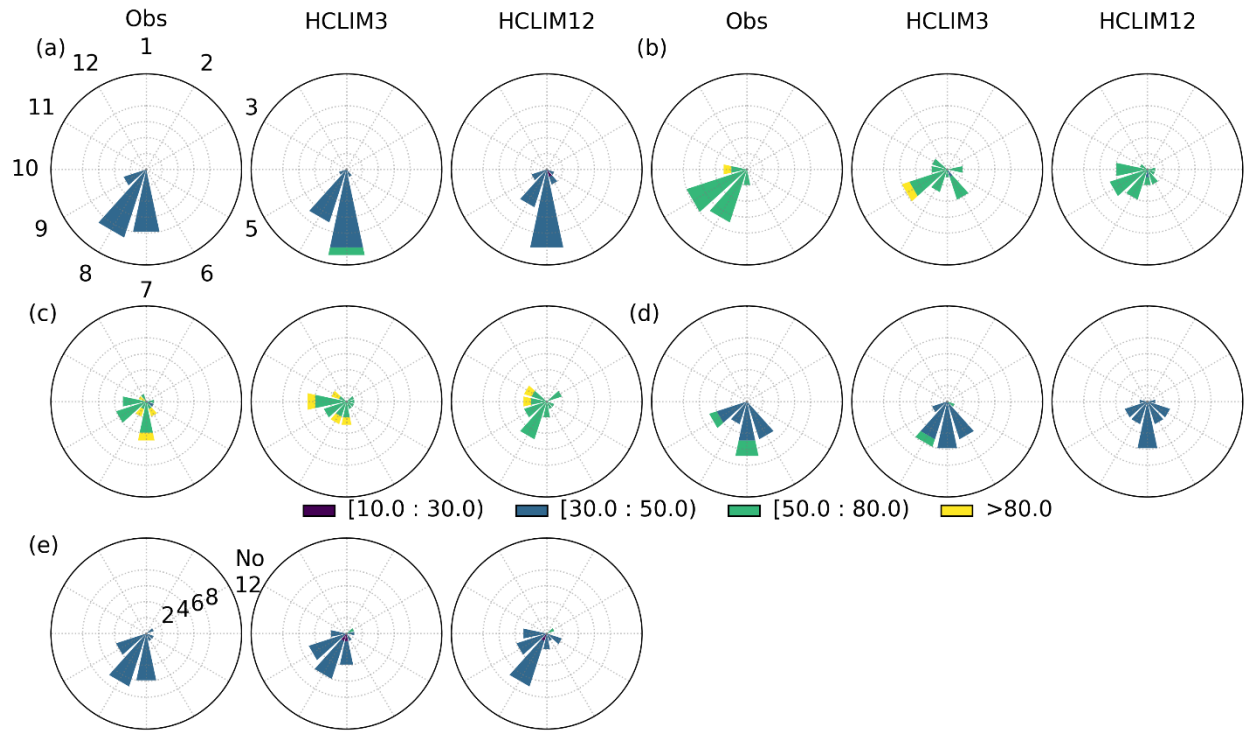393 **August; Autumn: September, October, November.**

394

Figure 10: The seasonality of frequency and magnitude of Rx1d precipitation from the in-situ observation, HCLIM3 and
HCLIM12 during 1999-2018 over different regions: a) Eastern, b) South, c) West, d) Middle, f) North. The color
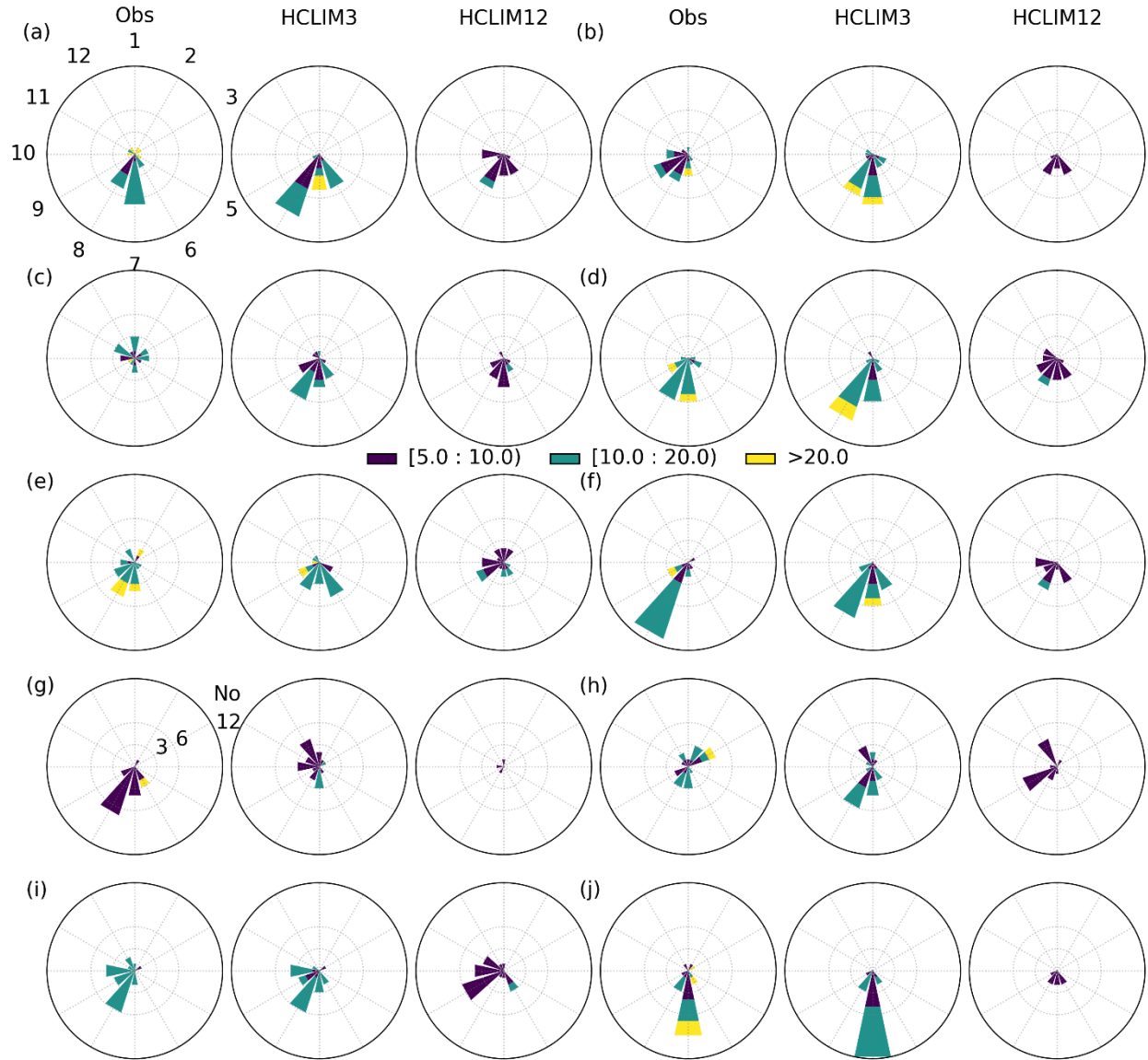represents the magnitude of Rx1d (m³/s).

398

Figure 11: Seasonality of the frequency and magnitude of Rx1h precipitation from the in-situ, HCLIM3 and HCLIM12 during 1999-2018 at 10 rain gauge stations (Table S1), i.e., a) Østre Toten - Apelsvoll, b) Kvithamar, c) Stryn - Kroken, d) Ås - Rustadskogen, e) Særheim, f) Kise in Hedmark, g) Tromsø – Holt, h) Tjøtta, i) Fureneset, j) Løken i Volbu. The color represents the magnitude of Rx1h (m^3/s).

Figure 9 and Figure 10 show the comparison of seasonality (indicated by monthly distribution) of annual Rx1d (e.g., frequency and magnitude) from both HCLIM3 and HCLIM12, compared to SeNorge and in-situ observation, respectively. From the seasonality of observed daily extreme precipitation in Fig. 9, we can see that winter-autumn precipitation dominates in almost all regions, except the middle and northern regions, where spring-summer precipitation is more prevalent. HCLIM3 captures the seasonality of Rx1d frequency at the regional scale in most regions except in middle region, where winter-autumn precipitation dominates. In contrast, HCLIM12 performs poorly in the eastern and middle regions. It is particularly noteworthy that HCLIM3 has an enhanced ability to capture the seasonality of extreme precipitation frequency over the western region compared to HCLIM12. Heavy

413   precipitation over 50 mm/day occurs mainly in the south and west, which is also simulated by HCLIM3 and

414   HCLIM12. In general, both HCLIM3 and HCLIM12 demonstrate competence in capturing the magnitude of

415   extreme daily precipitation seasonally at regional scale in most regions except middle region.

416   The seasonal performance of Rx1d from HCLIM3 and HCLIM12 in the local scale is also confirmed by the in-

417   situ observation, as shown in Fig. 10. A larger magnitude of annual Rx1d across five regions at local scale than

418   regional scale is shown for observation, HCLIM3 and HCLIM12. Generally, spring-summer precipitation events are

419   more frequent in the east, middle and north, while winter-autumn events are frequent in the south and west, and both

420   HCLIM3 and HCLIM12 capture this pattern well. In comparison, HCLIM3 better represents the seasonality of

421   frequency in the south, west and middle, compared to HCLIM12. For the seasonality of annual Rx1d at local scale,

422   as shown in Fig. 11, HCLIM3 more accurately represents the seasonality of Rx1h compared to HCLIM12, which

423   tends to underestimate the frequency of hourly extremes in most sites. Compared with RCMs, CPRCMs demonstrate

424   better potential performance in simulating seasonality of extreme precipitation, with particularly improved accuracy

425   for the hourly extremes at the local scale.

426 **4.5 Orographic effect on seasonal extreme precipitation**

427 **4.5.1 Seasonal Rx1d at regional scale**
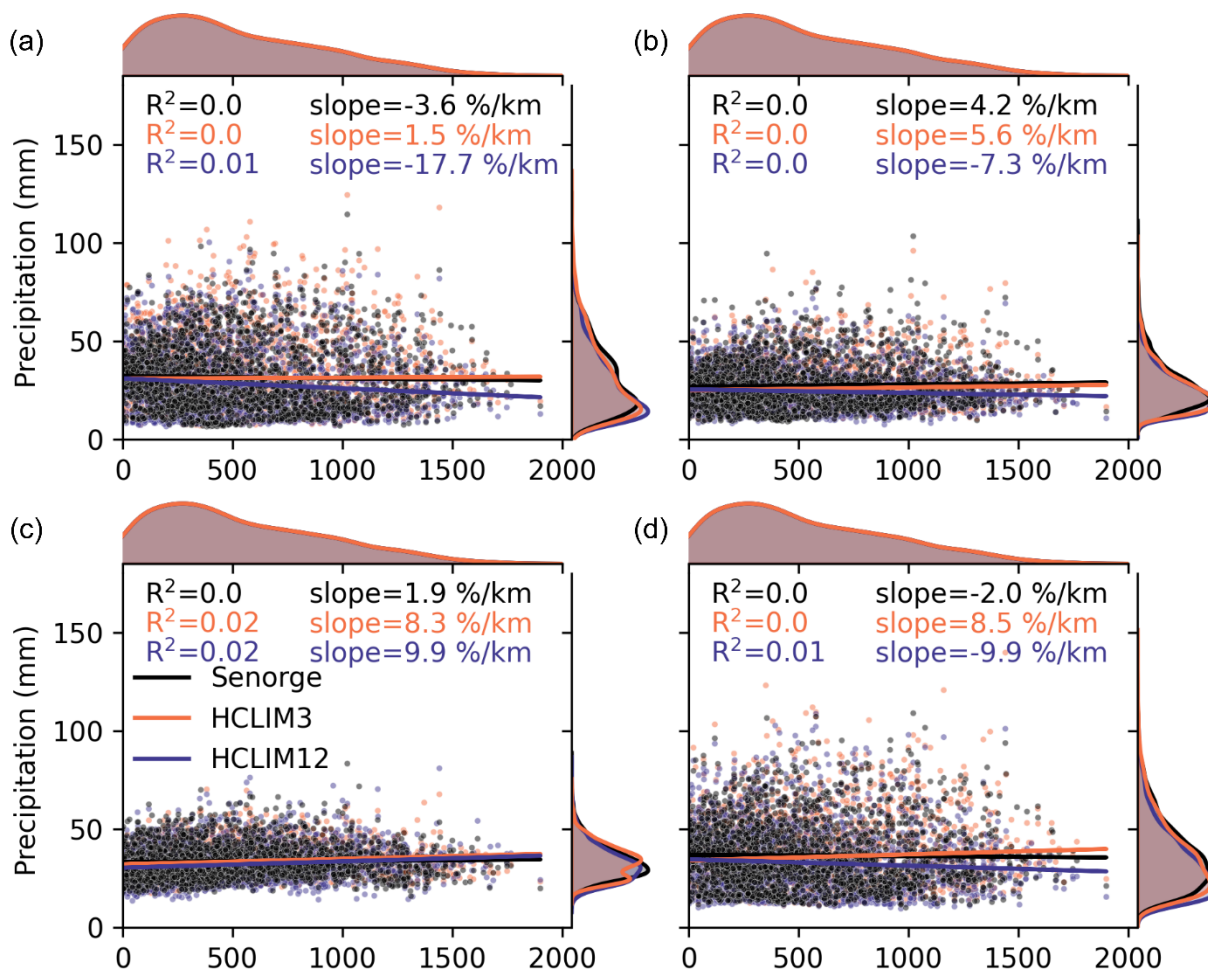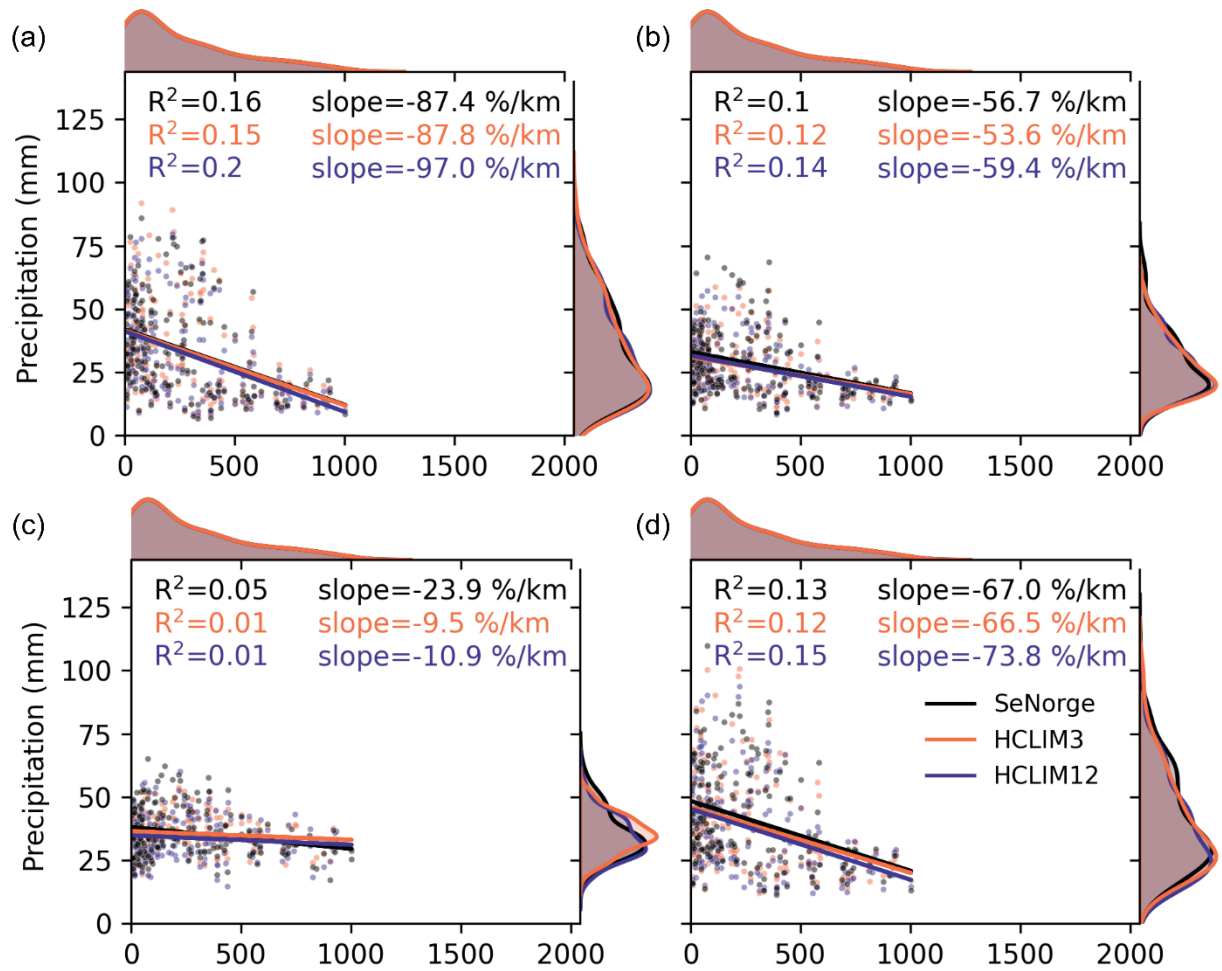

428
429 **Figure 12: Relationship between elevation and Rx1d (maximum 1-day precipitation) for (a) winter, (b) spring, (c)**
430 **summer, and (d) autumn, as derived from SeNorge and HCLIMs (i.e., HCLIM3 and HCLIM12) across mainland Norway**
431 **during the period of 1999-2018.**
432

433   The relationship of seasonal Rx1d with elevation from SeNorge, HCLIM3 and HCLIM12 is shown in Fig. 12.

434   Compared to HCLIM12, HCLIM3 more accurately captures the no evident linear relation (indicated by zero

435   coefficient of determination R^2) of seasonal Rx1d with elevation, similar to SeNorge, though it depicts a more

436   pronounced increase with elevation than SeNorge during summer. For example, both HCLIM3 and HCLIM12

437   simulate a large average increase in summer Rx1d with elevation (over 8 %/km), compared to observation, as

438   indicated by the larger absolute slope values. Generally, SeNorge, HCLIM3 and HCLIM12 showed the weak

439   relationship of seasonal Rx1d with altitude.

440   **4.5.2 Seasonal Rx1d at local scale**

441

Figure 13: Relationship between elevation and Rx1d (maximum 1-day precipitation) for (a) winter, (b) spring, (c) summer, and (d) autumn, based on daily in-situ observation and HCLIMs (i.e., HCLIM3 and HCLIM12) across mainland Norway during the period of 1999-2018.

445

446   Figure 13 represents the relationship of the seasonal Rx1d from in-situ observation, HCLIM3 and HCLIM12 with

447   elevation at local scale. The observed reverse orographic effect, seasonal Rx1d decrease with elevation, clearly

448   depicts with an average decrease of winter, spring, summer and autumn Rx1d of more than 87.4%, 56.7%, 23.9%

449   and 67% per kilometer. HCLIM3 more accurately represents the observed orographic influences on Rx1d in all

450   seasons except summer than HCLIM12. Moreover, HCLIM12 displays a more pronounced decline in Rx1d with

451   elevation, as evidenced by a steeper slope, across all seasons except summer, when compared to observation.

452   Generally, the reverse orographic effect is shown for the Rx1d from in-situ observation, HCLIM3 and HCLIM12.
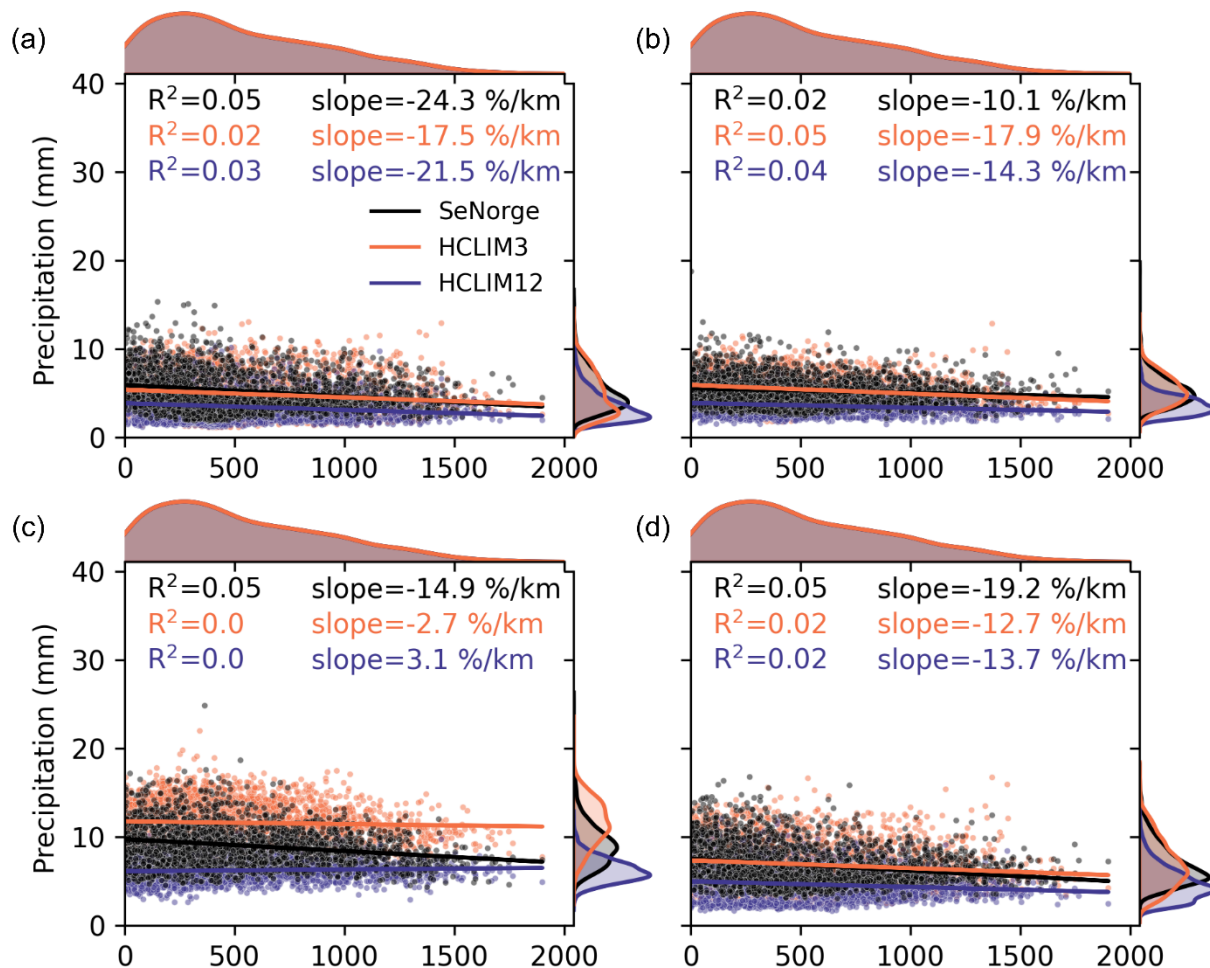
4.5.3 Seasonal Rx1h at regional scale

Figure 14: Relationship between elevation and Rx1h (maximum 1-hour precipitation) for (a) winter, (b) spring, (c) summer, and (d) autumn, as derived from SeNorge2 and HCLIMs (i.e., HCLIM3 and HCLIM12) across mainland Norway during the period of 2010-2018.

The relationship of seasonal Rx1h with elevation from gridded observation (SeNorge2) and simulation is further explored, as shown in Fig. 14. The reverse orographic effect of SeNorge2 on Rx1h was manifested in all seasons, with average decreases exceeding 24.3%, 10.1%, 14.9% and 19.2% per kilometer in winter, spring, summer and autumn, respectively. Compared to HCLIM12, HCLIM3 more accurately captures the decrease in seasonal Rx1h with elevation during winter, summer and autumn, though it still underestimates the decrease rate relative to observation. By contrast, HCLIM12 can only reflect the similar reverse orographic on Rx1h with observation in spring. The density plots of Rx1h reveal a dry bias in HCLIM12, particularly noticeable in summer, where it inversely correlates Rx1h with elevation.

5 Discussion

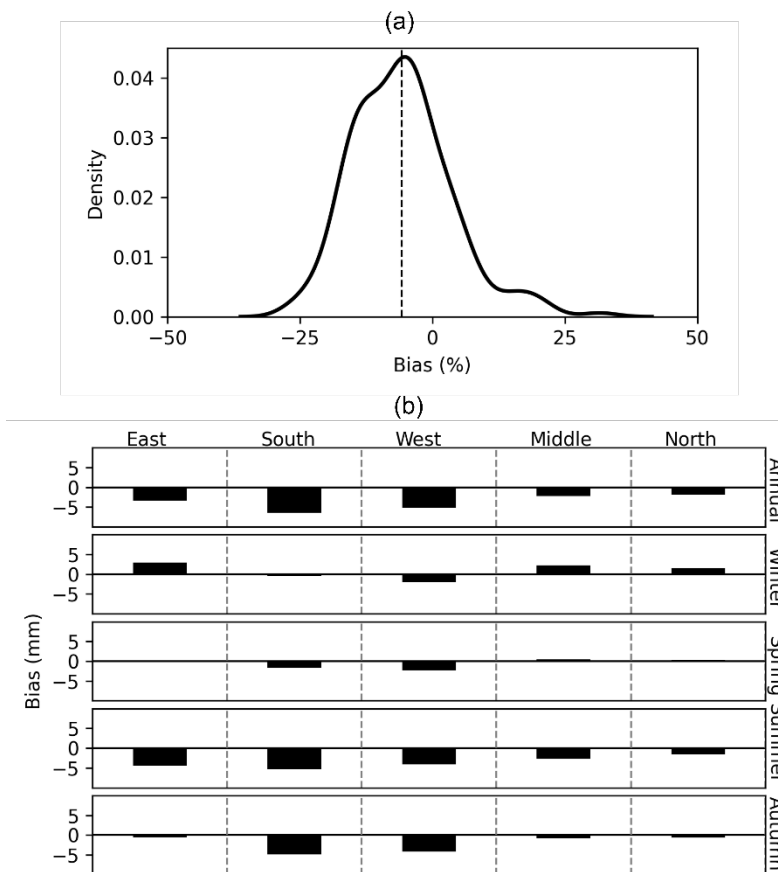## 5.1 Comparison between SeNorge vs in-situ observation

Figure 15: (a) Density distribution of bias for Rx1d between SeNorge and daily in-situ observations from 194 stations during 1999-2018; (b) the percentage difference of seasonal Rx1d between SeNorge and daily in-situ observations across the five regions. The bias is calculated as the SeNorge minus daily in-situ observations at each grid-point.

To further explore the uncertainty of different observation datasets on local scale model evaluation, we investigate the bias of SeNorge's annual and seasonal Rx1d from daily in-situ observations (see in Fig. 15). Our analysis in the Fig.15 (a) shows that SeNorge mostly underestimates the annual Rx1d compared to in-situ observation at 192 stations, with an average bias of -5.8% and a range between -28% and 25%. Although SeNorge data are designed to improve hydrological simulations (Lussana et al., 2019), their dry-biases still persist in most seasons and regions, especially in summer. It is noteworthy that SeNorge slightly overestimates the winter Rx1d in eastern, middle and northern regions. Moreover, SeNorge underestimates the return levels of Rx1d for different return periods (e.g., 5-, 10-, 20- and 50-year) in all regions (Fig. S3).

The larger differences between SeNorge and in-situ observation in simulating the Rx1d are manifested in the annual summer and autumn in the south and west, and in the summer in the east, where SeNorge tends to underestimate Rx1d more than in-situ observation. This discrepancy helps explain the differences between HCLIM3's performance in simulating Rx1d in summer in the east and autumn in the south and west at regional scale, compared to the local scale, as shown in Fig. 2 (c) and Fig. 5 (c). Generally, the difference between SeNorge

487 and in-situ observation at daily scale is not very large, which is why in most regions the added value of HCLIM3 in

488 Rx1d at the regional scale is similar to that at the local scale. However, it should be noted that the interpolated

489 precipitation from SeNorge may introduce uncertainties in assessing the performance of CPRCM at the local scale

490 due to the sparse distribution of daily and hourly rain-gauges at high altitude. Especially, for the hourly extremes at

491 the local scale and regional scales, larger uncertainties should be considered due to the limited data from only ten

492 rain-gauges at local scales and nine-years of data series at the regional scale. The impact of station density on the

493 errors of gridded datasets were also highlighted by Gervais et al. (2014b), who suggested that low station density is

494 an important source of errors in such datasets. To address these challenges and enhance the accuracy of extreme

495 precipitation assessments, future studies should prioritize expanding in-situ datasets and improving the spatial

496 coverage of observational networks, especially at the 1-hour timescale.

497 **5.2 Added value of CPRCMs at regional scale**

498 HCLIM3 demonstrates clear advantages over HCLIM12 in capturing the annual Rx1d in most regions. In terms of

499 regional averages, HCLIM12 underestimates Rx1d in most regions except the east and is biased towards wetter,

500 while HCLIM3 shows relatively smaller biases in most regions except the east, due to improvements in

501 microphysics and convection schemes (Lind et al., 2020).

502 Despite the overall better performance of HCLIM3, slightly larger biases in summer over the east, south and

503 west may result from the model's sensitivity to convective processes and limitations in accurately resolving

504 localized dynamics under moisture-rich and unstable atmospheric conditions. These challenges are particularly

505 pronounced during summer, when the intensity of convective activity increases, leading to rapid atmospheric

506 feedbacks and localized extremes (Poujol et al., 2021). In contrast, the southern region in winter is mainly affected

507 by atmospheric rivers (ARs) associated to extratropical cyclones, and HCLIM3 can better capture this feature due to

508 its finer resolution.

509 In terms of annual Rx1h, HCLIM3 outperforms HCLIM12, although it exhibits a wet bias compared to

510 SeNorge2. HCLIM12 underestimates Rx1h in most grids, likely due to its reliance on parameterization schemes that

511 fail to capture extremes (Médus et al., 2022). However, HCLIM3 shows larger biases in seasonal Rx1h in the west

512 in all seasons except spring, and in the east and middle region in summer, the overestimation of HCLIM3 over

513 Norway may be attributed to the underestimation in the hourly SeNorge2 (Lussana et al., 2018). Compared with

514 daily extremes, both HCLIM3 and HCLIM12 exhibit larger biases in simulating hourly extremes compared to daily

515 extremes, both at the annual and seasonal scales. It is important to note the limitations of the SeNorge2 dataset,

516 which only spans eight years and is interpolated from sparse hourly rain gauges.

517 In summary, HCLIM3 demonstrates better agreement with observations across most regions of Norway and

518 seasons at the regional scale, with the exception of the east and summer. This is consistent with previous studies

519 highlighting the advantage of convection-permitting models, especially in capturing extreme precipitation events

520 over complex terrain (Kendon et al., 2023; Médus et al., 2022; Lucas-Picher et al., 2021).

5.3 Added value of CPRCMs at local scale

The analysis of local scale convection-permitting climate models (CPRCMs) highlights their better performance in capturing precipitation extremes. HCLIM3 demonstrates notable advantages over HCLIM12, especially in terms of hourly precipitation extremes (Rx1h). For example, HCLIM3 achieves near-zero bias for the annual Rx1d in Norway (Fig. 5) and relative smaller bias for hourly extremes (Fig. 7 and Fig. 8) in all stations, while HCLIM12 consistently underestimates the return levels for hourly extremes at most station (Fig. 8) and daily extremes in all regions. Médus et al. (2022) also pointed out that RCMs underestimate the return levels of Rx1h in Norway. Thomassen et al. (2023) compared the performance of HCLIM3 and HCLIM12 based on local rain-gauge data in Denmark, and found that HCLIM12 indeed underestimate the hourly extreme event and HCLIM3 agree well with observation. Despite these benefits, the added value of HCLIM3 is not uniform across all stations and seasons, which struggle to capture summer daily extremes in the south and west, and the return level in the east and west. However, it should also be noted that the analysis is based on data from only 10 sites, which limits the generalizability of the findings to local hourly extreme events. Further studies of hourly extreme events at more stations are needed to validate these results and provide a more comprehensive understanding. Additionally, the uncertainties in the extreme precipitation analysis based on the stationary GEV method with a 20-years data series should also be noted.

The added value of CPRCMs in simulating hourly precipitation extremes is more obvious at the local scale than at the regional scale. The damped extremes caused by grid-scale averaging may explain the smaller return-level observed for HCLIM3 and HCLIM12 compared to station-level observations. As discussed in Section 5.1, this discrepancy between regional and local scales may be partly due to the inadequate density of in-situ observations.

Few studies have systematically compared hourly and daily rainfall in RCMs due to the challenges in reliably simulating hourly extremes. In line with Ban et al. (2014), we find that RCMs such as HCLIM12 demonstrate reasonably well performance for daily extremes with biases less than 50%. However, CPRCMs such as HCLIM3 perform better for hourly extremes. This is consistent with previous studies (Jiang et al., 2013; Thomassen et al., 2023), such as, Jiang et al. (2013), which showed that it is challenging to capture sub-daily extreme rainfall using RCMs with a resolution of 10 km in the southwestern United States. The better performance of CPRCMs compared to RCMs at hourly scale is consistent with the findings by Médus et al. (2022) and Ban et al. (2014), emphasizing that the CPRCMs have significantly better sub-daily precipitation characteristics, including spatial distribution and duration-intensity characteristics. Nonetheless, further improvements in the observation networks and longer observational datasets are necessary to fully verify and realize the benefits of CPRCMs at finer spatial and temporal scales.

Comparison of regional and local extreme precipitation seasonality confirms that HCLIM3 is able to represent the seasonality of daily extremes, although both HCLIM3 and HCLIM12 fail to capture the spring-summer events in the middle region. Moustakis et al. (2021) also highlighted the adequacy of CPRCMs (CTL-WRF~4 km) in capturing seasonality observed over the United States. In particular, we observe HCLIM3 better represent the seasonality of hourly precipitation at the local scale. The persistent underestimation of hourly extremes by

557 HCLIM12 may be attributed to higher uncertainty in its convective parameterization scheme or numerical
558 uncertainties at the local scale.

5.4 Added value of CPRCMs in reproducing reverse orographic effect

560 An unclear relation of daily extreme precipitation with elevation was also seen from the study of Dallan et al.
561 (2023), in which, they analyzed annual daily return level based on CPRCMs and in-situ observation over Alpine
562 region. By comparing the relationship between elevation and seasonal variation of extreme precipitation, HCLIM3
563 represents the reverse orographic effect well at regional and local scale, although there is a weak relationship
564 between extreme precipitation and elevation at the regional scale. The reverse orographic effects on hourly and daily
565 extremes vary with seasons, indicating the influence of topography on extreme precipitation at different timescales
566 and emphasizing the reliability of simulation of extreme precipitation over complex terrain. Unlike Rx1d at the
567 regional scale, which is less affected by topography, the slope of the reverse orographic effect of daily extreme
568 precipitation at the local scale is more clearly. From a seasonal perspective, the reverse orographic effect of extreme
569 precipitation in summer is not well captured in HCLIM3 and HCLIM12, which may be related to the intense
570 orographically-sustained convection affected by the atmospheric, aerosol conditions, local terrain slope and
571 shadowing effects, which RCMs and CPRCMs fail to capture (Dallan et al., 2023; Poujol et al., 2021).
572   For hourly extremes, the reverse orography effect of seasonal Rx1h in this study is consistent with the reverse
573 orographic effect of hourly return level, as found by Dallan et al. (2023) over Alpine region. HCLIM3 and
574 HCLIM12 well capture the reverse orography effect on seasonal Rx1h, especially in HCLIM3, although a stronger
575 decrease of Rx1h with elevation is observed from SeNorge2 except spring. In comparison, lower Rx1h and weak
576 reverse orography effect is found in HCLIM12 in all seasons. Our findings confirm the reverse orographic effect on
577 Rx1h, as demonstrated by Marra et al. (2021) for hourly precipitation and Formetta et al. (2022) for sub-hourly
578 scale.
579   Furthermore, we demonstrate the reverse orographic effect for both seasonal Rx1h and Rx1d, which contrasts
580 with the findings of Formetta et al. (2022), who identified a reverse orographic effect for hourly and sub-hourly
581 durations, and an orographic enhancement for durations of approximately 8 hours or longer. The "orographic
582 enhancement" (Avanzi et al., 2021; Formetta et al., 2022; Amponsah et al., 2022)—the increase in precipitation on
583 the windward side due to the lifting of air masses and the decrease on the leeward side from air descent and
584 drying—is not found in our study at either the regional or local scales. These results deviate from the anticipated
585 patterns, which may be attributed to the combined effects of latitude, climate, altitude zones, static atmospheric or
586 aerosol conditions, and shadowing effects (Amponsah et al., 2022; Napoli et al., 2019).
587   It should be noted that simple relationship between extreme precipitation and elevation is difficult to build due
588 to several land surface characteristics could influence the precipitation, a complex regression model should be
589 considered to more realistically quantify the reverse orographic effect (Zhang et al., 2018) in the future. The
590 interpolated gridded dataset and limited rain gauges over the complex orography, along with the decreasing station
591 density at higher elevations, may also limit the reliable analysis of the reverse orographic effect. The sparsity of rain

592 gauges and under catch problems could also lead to underestimation of precipitation, especially in the complex

593 orography (Lussana et al., 2018, 2019; Gervais et al., 2014b).

594 **6 Conclusions**

595 In this study, we conducted a comprehensive evaluation of extreme precipitation characteristics from regional to

596 local scale in Norway, focusing on five distinct regions, utilizing a convection-permitting regional climate model

597 (HCLIM3) and comparing it with its convection-parameterized regional climate model (HCLIM12) forced by ERA-

598 Interim data during 1999-2018.

599 The key conclusions of this study are as follows:

600 a) At regional scale, HCLIM3 shows consistent advantage in capturing Rx1d, compared to HCLIM12, with

601 improved representation of Rx1d in most regions and season, while HCLIM12 underestimates the annual

602 daily extremes in all regions except the east. Specifically, HCLIM3 shows larger bias of Rx1d in summer

603 over east, south and west regions, and the return level of daily extreme in the eastern region. In

604 comparison, for hourly extremes, HCLIM3 captures Rx1h better in most regions and seasons except the

605 west and the summer compared to HCLIM12. In general, HCLIM3 overestimates the annual Rx1h while

606 HCLIM12 underestimates it. Besides, HCLIM3 and HCLIM12 show larger bias in percentage for hourly

607 extremes than daily extremes.

608 b) At local scale, HCLIM3 shows added value in capturing the annual and seasonal Rx1d in most regions,

609 compared to HCLIM12. Specifically, HCLIM3 can better capture the return levels of daily extremes in

610 most regions except in the west and east, and it shows smaller biases in Rx1d across Norway for all

611 seasons, except summer in the southern and western regions. Overall, HCLIM3 shows consistent benefit

612 in capturing the daily extremes in the middle and north regions compared with HCLIM12, both at the

613 regional and local scales. For hourly extreme precipitation, HCLIM3 outperforms HCLIM12 in capturing

614 the annual Rx1h and return levels in those 10 stations.

615 c) For the seasonality of extremes, at the regional scale, HCLIM3 and HCLIM12 can well characterize the

616 seasonality of daily extremes except for the middle region, especially for HCLIM3 in the western region.

617 At local scale, the seasonality of Rx1d can also be captured by HCLIM3 and HCLIM12. A distinct

618 advantage emerges with HCLIM3 for hourly extremes, where it accurately reflects both the occurrence

619 and intensity of these events across different seasons, while HCLIM12 tends to underestimate these

620 aspects.

621 d) In Norway, the effect of the preserved topography on seasonal Rx1h and Rx1d emerge from regional to

622 local scales, although weak relationship between Rx1d and elevation is demonstrated at regional scale. For

623 seasonal Rx1h, both HCLIM3 and HCLIM12 can capture the reverse orographic effect at regional scale,

624 but no added value is shown in HCLIM3. In particular, at the local scale, the reverse orographic effect of

625 seasonal Rx1d is more pronounced, and HCLIM3 provides added value in all seasons except summer.

635   **References**

636   Adinolfi, M., Raffa, M., Reder, A., and Mercogliano, P.: Evaluation and Expected Changes of Summer Precipitation
637   at Convection Permitting Scale with COSMO-CLM over Alpine Space, 10.3390/atmos12010054, 2021.

638   Amponsah, W., Dallan, E., Nikolopoulos, E. I., and Marra, F.: Climatic and altitudinal controls on rainfall extremes
639   and their temporal changes in data-sparse tropical regions. Journal of Hydrology 612, 128090.
640   https://doi.org/10.1016/j.jhydrol.2022.128090, 2022.

641   Avanzi, F., Ercolani, G., Gabellani, S., Cremonese, E., Pogliotti, P., Filippa, G., Morra di Cella, U., Ratto, S.,
642   Stevenin, H., Cauduro, M., and Juglair, S.: Learning about precipitation lapse rates from snow course data
643   improves water balance modeling, Hydrol. Earth Syst. Sci., 25, 2109-2131, 10.5194/hess-25-2109-2021,
644   2021.

645   Ban, N., Schmidli, J., and Schär, C.: Evaluation of the convection-resolving regional climate modeling approach in
646   decade-long simulations, Journal of Geophysical Research: Atmospheres, 119, 7889-7907,
647   https://doi.org/10.1002/2014JD021478, 2014.

648   Ban, N., Rajczak, J., Schmidli, J., and Schär, C.: Analysis of Alpine precipitation extremes using generalized
649   extreme value theory in convection-resolving climate simulations, Climate Dynamics, 55, 61-75,
650   10.1007/s00382-018-4339-4, 2020.

651   Chapman, S., Bacon, J., Birch, C. E., Pope, E., Marsham, J. H., Msemo, H., Nkonde, E., Sinachikupo, K., and
652   Vanya, C.: Climate Change Impacts on Extreme Rainfall in Eastern Africa in a Convection-Permitting
653   Climate Model, Journal of Climate, 36, 93-109, https://doi.org/10.1175/JCLI-D-21-0851.1, 2023.

654   Coles, S., Pericchi, L. R., and Sisson, S.: A fully probabilistic approach to extreme rainfall modeling, Journal of
655   Hydrology, 273, 35-50, https://doi.org/10.1016/S0022-1694(02)00353-0, 2003.

656   Dallan, E., Marra, F., Fosser, G., Marani, M., Formetta, G., Schär, C., and Borga, M.: How well does a convection-
657   permitting regional climate model represent the reverse orographic effect of extreme hourly precipitation?,
658   Hydrol. Earth Syst. Sci., 27, 1133-1149, 10.5194/hess-27-1133-2023, 2023.

659   Di Piazza, A., Conti, F. L., Noto, L. V., Viola, F., and La Loggia, G.: Comparative analysis of different techniques
660   for spatial interpolation of rainfall data to create a serially complete monthly time series of precipitation for

Sicily, Italy, International Journal of Applied Earth Observation and Geoinformation, 13, 396-408, https://doi.org/10.1016/j.jag.2011.01.005, 2011.

Dyrrdal, A. V., Médus, E., Dobler, A., Hodnebrog, Ø., Arnbjerg-Nielsen, K., Olsson, J., Thomassen, E. D., Lind, P., Gaile, D., and Post, P.: Changes in design precipitation over the Nordic-Baltic region as given by convection-permitting climate simulations, Weather and Climate Extremes, 42, 100604, 10.1016/j.wace.2023.100604, 2023.

Formetta, G., Marra, F., Dallan, E., Zaramella, M., and Borga, M.: Differential orographic impact on sub-hourly, hourly, and daily extreme precipitation. Advances in Water Resources 159, 104085. https://doi.org/10.1016/j.advwatres.2021.104085, 2022.

Gervais, M., Gyakum, J. R., Atallah, E., Tremblay, L. B., and Neale, R. B.: How Well Are the Distribution and Extreme Values of Daily Precipitation over North America Represented in the Community Climate System Model? A Comparison to Reanalysis, Satellite, and Gridded Station Data, Journal of Climate, 27, 5219-5239, https://doi.org/10.1175/JCLI-D-13-00320.1, 2014a.

Gervais, M., Tremblay, L. B., Gyakum, J. R., and Atallah, E.: Representing Extremes in a Daily Gridded Precipitation Analysis over the United States: Impacts of Station Density, Resolution, and Gridding Methods, Journal of Climate, 27, 5201-5218, https://doi.org/10.1175/JCLI-D-13-00319.1, 2014b.

Giordani, A., Cerenzia, I. M. L., Paccagnella, T., and Di Sabatino, S.: SPHERA, a new convection-permitting regional reanalysis over Italy: Improving the description of heavy rainfall, Quarterly Journal of the Royal Meteorological Society, 149, 781-808, https://doi.org/10.1002/qj.4428, 2023.

Jiang, P., Gautam, M. R., Zhu, J., and Yu, Z.: How well do the GCMs/RCMs capture the multi-scale temporal variability of precipitation in the Southwestern United States?, Journal of Hydrology, 479, 75-85, https://doi.org/10.1016/j.jhydrol.2012.11.041, 2013.

Kendon, E. J., Fischer, E. M., and Short, C. J.: Variability conceals emerging trend in 100yr projections of UK local hourly rainfall extremes, Nature Communications, 14, 1133, 10.1038/s41467-023-36499-9, 2023.

Kendon, E. J., Stratton, R. A., Tucker, S., Marsham, J. H., Berthou, S., Rowell, D. P., and Senior, C. A.: Enhanced future changes in wet and dry extremes over Africa at convection-permitting scale, Nature Communications, 10, 1794, 10.1038/s41467-019-09776-9, 2019.

Kent, C., Dunstone, N., Tucker, S., Scaife, A. A., Brown, S., Kendon, E. J., Smith, D., McLean, L., and Greenwood, S.: Estimating unprecedented extremes in UK summer daily rainfall, Environmental Research Letters, 17, 014041, 10.1088/1748-9326/ac42fb, 2022.

Kim, Y., Rocheta, E., Evans, J. P., and Sharma, A.: Impact of bias correction of regional climate model boundary conditions on the simulation of precipitation extremes, Climate Dynamics, 55, 3507-3526, 10.1007/s00382-020-05462-5, 2020.

Knist, S., Goergen, K., and Simmer, C.: Evaluation and projected changes of precipitation statistics in convection-permitting WRF climate simulations over Central Europe, Climate Dynamics, 55, 325-341, 10.1007/s00382-018-4147-x, 2020.

697 Konstali, K. and Sorteberg, A.: Why has Precipitation Increased in the Last 120 Years in Norway?, Journal of
698   Geophysical Research: Atmospheres, 127, 10.1029/2021jd036234, 2022.
699 Li, J., Gan, T. Y., Chen, Y. D., Gu, X., Hu, Z., Zhou, Q., and Lai, Y.: Tackling resolution mismatch of precipitation
700   extremes from gridded GCMs and site-scale observations: Implication to assessment and future projection,
701   Atmospheric Research, 239, 104908, https://doi.org/10.1016/j.atmosres.2020.104908, 2020a.
702 Li, L., Pontoppidan, M., Sobolowski, S., and Senatore, A.: The impact of initial conditions on convection-permitting
703   simulations of a flood event over complex mountainous terrain, Hydrol. Earth Syst. Sci., 24, 771-791,
704   10.5194/hess-24-771-2020, 2020b.
705 Li, P., Furtado, K., Zhou, T., Chen, H., and Li, J.: Convection-permitting modelling improves simulated
706   precipitation over the central and eastern Tibetan Plateau, Quarterly Journal of the Royal Meteorological
707   Society, 147, 341-362, https://doi.org/10.1002/qj.3921, 2021.
708 Lind, P., Lindstedt, D., Kjellström, E., and Jones, C.: Spatial and Temporal Characteristics of Summer Precipitation
709   over Central Europe in a Suite of High-Resolution Climate Models, Journal of Climate, 29, 3501-3518,
710   https://doi.org/10.1175/JCLI-D-15-0463.1, 2016.
711 Lind, P., Belušić, D., Christensen, O. B., Dobler, A., Kjellström, E., Landgren, O., Lindstedt, D., Matte, D.,
712   Pedersen, R. A., Toivonen, E., and Wang, F.: Benefits and added value of convection-permitting climate
713   modeling over Fenno-Scandinavia, Climate Dynamics, 55, 1893-1912, 10.1007/s00382-020-05359-3,
714   2020.
715 Liu, C., Ikeda, K., Rasmussen, R., Barlage, M., Newman, A. J., Prein, A. F., Chen, F., Chen, L., Clark, M., Dai, A.,
716   Dudhia, J., Eidhammer, T., Gochis, D., Gutmann, E., Kurkute, S., Li, Y., Thompson, G., and Yates, D.:
717   Continental-scale convection-permitting modeling of the current and future climate of North America,
718   Climate Dynamics, 49, 71-95, 10.1007/s00382-016-3327-9, 2017.
719 Lucas-Picher, P., Argüeso, D., Brisson, E., Tramblay, Y., Berg, P., Lemonsu, A., Kotlarski, S., and Caillaud, C.:
720   Convection-permitting modeling with regional climate models: Latest developments and next steps. WIREs
721   Climate Change 12(6), e731. https://doi.org/10.1002/wcc.731, 2021.
722 Lussana, C., Tveito, O. E., Dobler, A., and Tunheim, K.: seNorge_2018, daily precipitation, and temperature
723   datasets over Norway, Earth Syst. Sci. Data, 11, 1531-1551, 10.5194/essd-11-1531-2019, 2019.
724 Lussana, C., Saloranta, T., Skaugen, T., Magnusson, J., Tveito, O. E., and Andersen, J.: seNorge2 daily
725   precipitation, an observational gridded dataset over Norway from 1957 to the present day, Earth Syst. Sci.
726   Data, 10, 235-249, 10.5194/essd-10-235-2018, 2018.
727 Mahoney, K., Ralph, F. M., Wolter, K., Doesken, N., Dettinger, M., Gottas, D., Coleman, T., and White, A.:
728   Climatology of Extreme Daily Precipitation in Colorado and Its Diverse Spatial and Seasonal Variability,
729   Journal of Hydrometeorology, 16, 781-792, https://doi.org/10.1175/JHM-D-14-0112.1, 2015.
730 Marra, F., Armon, M., Borga, M., and Morin, E.: Orographic Effect on Extreme Precipitation Statistics Peaks at
731   Hourly Time Scales, Geophysical Research Letters, 48, e2020GL091498,
732   https://doi.org/10.1029/2020GL091498, 2021.

733   Médus, E., Thomassen, E. D., Belušić, D., Lind, P., Berg, P., Christensen, J. H., Christensen, O. B., Dobler, A.,
734   Kjellström, E., Olsson, J., and Yang, W.: Characteristics of precipitation extremes over the Nordic region:
735   added value of convection-permitting modeling, Nat. Hazards Earth Syst. Sci., 22, 693-711, 10.5194/nhess-
736   22-693-2022, 2022.
737   Michel, C., Sorteberg, A., Eckhardt, S., Weijenborg, C., Stohl, A., and Cassiani, M.: Characterization of the
738   atmospheric environment during extreme precipitation events associated with atmospheric rivers in Norway
739   - Seasonal and regional aspects, Weather and Climate Extremes, 34, 100370, 10.1016/j.wace.2021.100370,
740   2021.
741   Moustakis, Y., Papalexiou, S. M., Onof, C. J., and Paschalis, A.: Seasonality, Intensity, and Duration of Rainfall
742   Extremes Change in a Warmer Climate, Earth's Future, 9, e2020EF001824,
743   https://doi.org/10.1029/2020EF001824, 2021.
744   Napoli, A., Crespi, A., Ragone, F., Maugeri, M., and Pasquero, C.: Variability of orographic enhancement of
745   precipitation in the Alpine region. Scientific Reports 9(1), 13352. 10.1038/s41598-019-49974-5, 2019.
746   Piani, C., Weedon, G. P., Best, M., Gomes, S. M., Viterbo, P., Hagemann, S., and Haerter, J. O.: Statistical bias
747   correction of global simulated daily precipitation and temperature for the application of hydrological
748   models, Journal of Hydrology, 395, 199-215, https://doi.org/10.1016/j.jhydrol.2010.10.024, 2010.
749   Pontoppidan, M., Kolstad, E. W., Sobolowski, S., and King, M. P.: Improving the Reliability and Added Value of
750   Dynamical Downscaling via Correction of Large-Scale Errors: A Norwegian Perspective, Journal of
751   Geophysical Research: Atmospheres, 123, 11,875-811,888, 10.1029/2018jd028372, 2018.
752   Poujol, B., Mooney, P. A., and Sobolowski, S. P.: Physical processes driving intensification of future precipitation
753   in the mid- to high latitudes, Environmental Research Letters, 16, 034051, 10.1088/1748-9326/abdd5b,
754   2021.
755   Prein, A. F., Langhans, W., Fosser, G., Ferrone, A., Ban, N., Goergen, K., Keller, M., Tölle, M., Gutjahr, O., Feser,
756   F., Brisson, E., Kollet, S., Schmidli, J., van Lipzig, N. P. M., and Leung, R.: A review on regional
757   convection-permitting climate modeling: Demonstrations, prospects, and challenges, Reviews of
758   Geophysics, 53, 323-361, https://doi.org/10.1002/2014RG000475, 2015.
759   Reder, A., Raffa, M., Montesarchio, M., and Mercogliano, P.: Performance evaluation of regional climate model
760   simulations at different spatial and temporal scales over the complex orography area of the Alpine region,
761   Natural Hazards, 102, 151-177, 10.1007/s11069-020-03916-x, 2020.
762   Rossi, M. W., Anderson, R. S., Anderson, S. P., and Tucker, G. E.: Orographic Controls on Subdaily Rainfall
763   Statistics and Flood Frequency in the Colorado Front Range, USA, Geophysical Research Letters, 47,
764   e2019GL085086, https://doi.org/10.1029/2019GL085086, 2020.
765   Tabari, H.: Climate change impact on flood and extreme precipitation increases with water availability, Scientific
766   Reports, 10, 13768, 10.1038/s41598-020-70816-2, 2020.
767   Thackeray, C. W., Hall, A., Norris, J., and Chen, D.: Constraining the increased frequency of global precipitation
768   extremes under warming, Nature Climate Change, 12, 441-448, 10.1038/s41558-022-01329-1, 2022.

769 Thomassen, E. D., Arnbjerg-Nielsen, K., Sørup, H. J. D., Langen, P. L., Olsson, J., Pedersen, R. A., and
770   Christensen, O. B.: Spatial and temporal characteristics of extreme rainfall: Added benefits with sub-
771   kilometre-resolution climate model simulations?, Quarterly Journal of the Royal Meteorological Society,
772   149, 1913-1931, https://doi.org/10.1002/qj.4488, 2023.
773 Wang, Y., Zhang, G. J., and He, Y.-J.: Simulation of Precipitation Extremes Using a Stochastic Convective
774   Parameterization in the NCAR CAM5 Under Different Resolutions, Journal of Geophysical Research:
775   Atmospheres, 122, 12,875-812,891, https://doi.org/10.1002/2017JD026901, 2017.
776 Zhang, T., Li, B., Yuan, Y., Gao, X., Sun, Q., Xu, L., and Jiang, Y.: Spatial downscaling of TRMM precipitation
777   data considering the impacts of macro-geographical factors and local elevation in the Three-River
778   Headwaters Region, Remote Sensing of Environment, 215, 109-127,
779   https://doi.org/10.1016/j.rse.2018.06.004, 2018.
780 Vormoor, K., Lawrence, D., Schlichting, L., Wilson, D., and Wong, W. K.: Evidence for changes in the magnitude
781   and frequency of observed rainfall vs. snowmelt driven floods in Norway, Journal of Hydrology, 538, 33-
782   48, 10.1016/j.jhydrol.2016.03.066, 2016.
783 Whan, K., Sillmann, J., Schaller, N., and Haarsma, R.: Future changes in atmospheric rivers and extreme
784   precipitation in Norway. Climate Dynamics 54(3), 2071-2084. 10.1007/s00382-019-05099-z, 2020.